Oxidation and Reconstructions of Alloy Model Catalysts

Platinum-Rhodium and Palladium-Gold

Edström, Helen

2023

Oxidation and Reconstructions of Alloy Model Catalysts

Platinum-Rhodium and Palladium-Gold

HELEN EDSTRÖM
DEPARTMENT OF PHYSICS | FACULTY OF SCIENCE | LUND UNIVERSITY

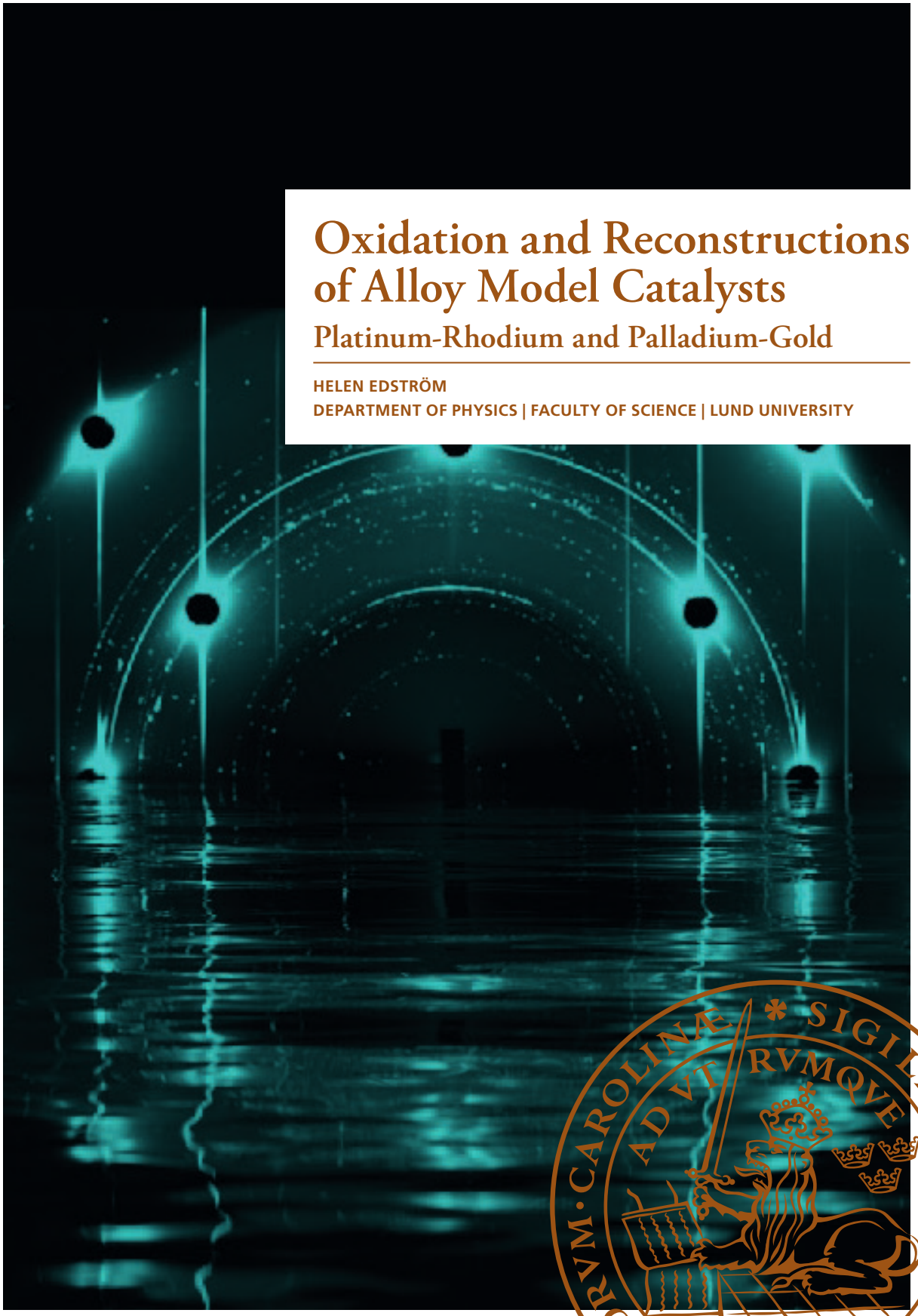

Oxidation and Reconstructions of Alloy Model Catalysts

Oxidation and Reconstructions of Alloy Model Catalysts

Platinum-Rhodium and Palladium-Gold

by Helen Edström

LUND
UNIVERSITY

Doctoral Thesis
Thesis advisors: Dr. Johan Gustafson, Prof. Edvin Lundgren
Faculty opponent: Prof. Christopher Nicklin

To be presented, with the permission of the Faculty of Science of Lund University, for public criticism in the Rydberg lecture hall at the Department of Physics 2023-12-08 at 13:15.

Organization
LUND UNIVERSITY

Department of Physics
Box 118
SE-221 00 LUND
Sweden

Document name
DOCTORAL DISSERTATION

Date of disputation
2023-12-08

Sponsoring organization

Author
Helen Edström

Title and subtitle
Oxidation and Reconstructions of Alloy Model Catalysts: Platinum-Rhodium and Palladium-Gold

Abstract
Alloys and bimetallic systems have shown many advantages in heterogeneous catalysis, but the details of their catalytic functions are not always known. For instance, the atomic details about surface reconstructions under catalytic reaction conditions, or which phases that are high-active or low-active. Furthermore, the model catalysts studied in laboratories often differ a lot from the industrial catalysts regarding working conditions and materials.

Surface reconstructions depend on surface science of both physical and chemical nature. Since catalytic reactions occur on the surface of catalysts, it is desirable to understand what happens at the atomic scale on the catalyst surface under reaction conditions. There are different techniques to study surfaces at the atomic level, regarding elemental composition as well as surface structure.

In this thesis, I have studied the surfaces of two alloy systems, PtRh and PdAu, under reaction conditions. CO oxidation over a $Pt_{25}Rh_{75}(100)$ single crystal was studied at a commissioning beamtime as a model system using HESXRD (Paper I and Paper II). Thin films of PdAu on a sapphire substrate, with varying Pd:Au ratios, has been oxidised, and the oxide formation and alloying process has been studied with HESXRD (Paper IV). Oxidation with subsequent reduction in methane has also been studied with APXPS (Paper V). I have also analysed the results from LEED, TPD, and TSD of CO oxidation over a Pd(100) single crystal (Paper III).

Two well-known oxygen structures were observed on the PtRh crystal: a (3×1) reconstruction with chemisorbed O and a $c(8 \times 2)$ surface oxide. Furthermore, an unexpected $c(2 \times 2)$ structure was observed under reducing conditions and elevated temperature. The quantitative analysis of these structures is presented in this thesis.

The PdAu oxidation experiment was a continuation of a methane oxidation study on a Pd(100) single crystal, showing that the catalytic activity decreases if the oxide grows too thick, but increases again upon oxide decomposition. It is believed that the thick oxide exposes the low-active (100) surface orientation while the thin oxide exposes the high-active (101) surface orientation. The idea with PdAu was to limit the amount of Pd that can be oxidised in order to keep the oxide thin and high-active. The changed lattice constant of PdAu compared to Pd, however, seems to stabilise the low-active PdO surface. We believe this can be helped by instead alloying Pd with Pt, or use PdAu samples with lower Au concentration.

Key words
Alloying, APXPS, Bimetallic Catalysts, Heterogeneous Catalysis, HESXRD, Oxidation, Oxide Formation, Palladium-Gold, Platinum-Rhodium, Surface Reconstruction

Classification system and/or index terms (if any)

Supplementary bibliographical information

Language
English

ISSN and key title

ISBN
978-91-8039-832-9 (print)
978-91-8039-831-2 (pdf)

Recipient's notes

Number of pages
153

Price

Security classification

Oxidation and Reconstructions of Alloy Model Catalysts

Platinum-Rhodium and Palladium-Gold

by Helen Edström

LUND
UNIVERSITY

Cover illustration front: Maximum intensity HESXRD image displaying the CTRs and c(2×2) SRs on a $Pt_{25}Rh_{75}(100)$ single crystal, taken at the Swedish High-Energy X-Ray Materials Science Beamline (P21.2) at PETRA III, DESY in Hamburg, Germany. Artistic image recreation by Kim Svensson.

Cover illustration back: And... he is alive! My lovely cat Fabian cosplaying as Schrödinger's cat.

Funding information: The thesis work was financially supported by The Knut and Alice Wallenberg Foundation and The Swedish Research Council.

Faculty of Science, Department of Physics

ISBN: 978-91-8039-832-9 (print)
ISBN: 978-91-8039-831-2 (pdf)

Printed in Sweden by Media-Tryck, Lund University, Lund 2023

Imagination is more important than knowledge.
Knowledge is limited. Imagination encircles the world.
Albert Einstein

Contents

List of Publications

This thesis is based on the following publications, referred to by their Roman numerals:

I **The (3×1) and c(8×2) Oxygen Structures Formed on a $Pt_{25}Rh_{75}$(100) Model Catalyst During CO Oxidation**
H. Edström, V. Vonk, L. Jacobse, H. Grönbeck, A. Schaefer, U. Hejral, S. Albertin, K. von Allmen, B. Hagman, E. Lundgren, C. Seitz, S. Geile, A. Stierle, and J. Gustafson
In manuscript

I performed data acquisition and analysis, participated in discussions about the DFT calculations, and was main responsible for the manuscript.

II **A c(2×2) Reconstruction of $Pt_{25}Rh_{75}$(100)**

V. Vonk, **H. Edström**, L. Jacobse, H. Grönbeck, A. Schaefer, U. Hejral, S. Albertin, K. von Allmen, B. Hagman, E. Lundgren, C. Seitz, S. Geile, A. Stierle, and J. Gustafson
In manuscript

I performed data acquisition and part of the analysis, participated in discussions about the rod simulations, and was main responsible for the manuscript.

III **Formation of Epitaxial PdO(100) During the Oxidation of Pd(100)**

V. Mehar, **H. Edström**, M. Shipilin, U. Hejral, C. Wu, A. Kadiri, S. Albertin, B. Hagman, K. von Allmen, T. Wiegmann, S. Pfaff, J. Drnec, J. Zetterberg, E. Lundgren, L. R. Merte, J. Gustafson, and J. F. Weaver
Journal of Physical Chemistry Letters 14 (2023) 8493 (7 pp)

I performed analysis of diffraction data, wrote a first draft manuscript, and gave feedback on the final manuscript.

IV **Alloying and Oxidation of PdAu Thin Films**

H. Edström, A. Schaefer, L. Jacobse, K. von Allmen, B. Hagman, P.-A. Carlsson, and J. Gustafson
Manuscript submitted to Thin Solid Films

I planned the experiments, performed data acquisition and analysis and was main responsible for the draft manuscript.

v **Oxidation of PdAu Thin Films and the Subsequent Reduction by CH_4 and Heat**

H. Edström, A. Schaefer, and J. Gustafson
In manuscript

I planned the experiments, performed data acquisition and analysis and was main responsible for the draft manuscript.

All papers are reproduced with permission of their respective publishers.

Publications not included in this thesis:

Oxygen induced faceting of Cu(911)

B. Hagman, A. Schaefer, **H. Edström**, K. von Allmen, and J. Gustafson
Surface Science 715 (2022) 121933 (4 pp)

Oxide growth on Cu(911)

B. Hagman, **H. Edström**, K. von Allmen, J. Gustafson, and A. Schaefer
In manuscript

CO_2 dissociation on Cu(911)

B. Hagman, **H. Edström**, J. Gustafson, A. Schaefer, A. Posada-Borbón, and H. Grönbeck
In manuscript

List of Acronyms

ALS	Advanced Light Source
APXPS	Ambient-Pressure X-Ray Photoelectron Spectroscopy
BC	Body Centered
BCC	Body Centered Cubic
CTR	Crystal Truncation Rod
CUS	Coordinatively Unsaturated
DESY	Deutsches Elektronen-Synchrotron
DFT	Density Functional Theory
D-S	Doniach-Šunjić
EBPVD	Electron-Beam Physical Vapour Deposition
ER	Eley-Rideal
ESCA	Electron Spectroscopy for Chemical Analysis
ESRF	European Synchrotron Research Facilitity
FCC	Face Centered Cubic
FWHM	Full Width at Half Maximum
GIXRD	Grazing Incidence X-Ray Diffraction
HCP	Hexagonal Closest Packed
HESXRD	High Energy Surface X-Ray Diffraction
IMFP	Inelastic Mean Free Path
LEED	Low Energy Electron Diffraction
LH	Langmuir-Hinshelwood
ML	Monolayer
MvK	Mars-van Krevelen
PD	Path Difference
Q.E.D.	*Quod Erat Demonstrandum* (”which was to be demonstrated”)
RDS	Rate-Determining Step
RLU	Reciprocal Lattice Unit
SC	Simple Cubic
SR	Surface Rod
SXRD	Surface X-Ray Diffraction
TPD	Temperature Programmed Desorption
TSD	Transmission Surface Diffraction
UHV	Ultra-High Vacuum
VASP	Vienna *Ab-initio* Simulation Package
XPS	X-Ray Photoelectron Spectroscopy

Acknowledgement

When I was deepest down in the dark abyss that is depression, I could never imagine that I could finish my thesis. How do you motivate your self to conduct a PhD project when you constantly have to try to motivate your self to keep living? When you feel your cognitive abilities slowly slipping away, leaving only fog behind... As I write this two years later, I feel like a whole new person, so far from the shadow figure I had turned into. No victory is too small to celebrate, and there are many people who deserve my thanks for enabling this thesis to see the (synchrotron) light of day.

First and foremost, I want to thank Pernilla Arvidsson, licensed psychotherapist at *Kävlingevägens Psykoterapi* in Lund. Without you, I would not be were I am today. You saw me when I could not see myself. You reminded me who I was before darkness devoured me, and made me believe I could be that person again. You sat by my side when my long-time suppressed emotions overwhelmed me, telling me that anxiety attacks never killed anyone. You took this wilted flower out of the shade to let it thrive in sunshine again. I wish I had met you when I was fourteen.

My supervisor Johan Gustafson, this is where I say thank you and I am sorry. I know I have not been the best PhD student, but you were always patient and diplomatic. The only thing I can say in my defence is that I was mentally ill, not even understanding it myself (I have learned the hard way to not underestimate normalisation processes). I guess we both did our best to get through these years. Also thanks to my co-supervisor Edvin Lundgren, for pleasant company on conferences and providing help when needed.

Thanks to my colleagues at the Division of Synchrotron Radiation, especially Kim von Allmen, Benjamin Hagman, Uta Hejral, and Stefano Albertin for help on beamtimes and other experimental help. Also thanks to Estephanía Lira, research engineer at the division, for experimental help and support. And thanks to Gary Harlow, for creating the HESXRD Analysis Toolkit (HAT), and especially for making it able to read .cbf files.

To colleagues at Chalmers University: Andreas Schaefer and Per-Anders Carlsson, for help on beamtimes; Henrik Grönbeck for help with DFT calculations and proof reading the DFT part of the thesis; John Andersson and Rosemary Brown for manufacturing the PdAu thin film samples (together with Andreas and Per-Anders). Also, thanks to everyone joining the KAW meetings with me, from both Chalmers University and Lund University. It was interesting to see what you work with, even when I did not understand everything.

We have had some collaboration with colleagues at DESY Nanolaboratory, to whom we owe thanks: Andreas Stierle, Vedan Vonk, and Leon Jacobse, for fruitful discussions about the PtRh(100) project. I got a lot of help with the softwares ANAROD (Vedran) and Igor Pro 8 (Leon), for which I am grateful. Also thanks to the research school HELIOS, where

I got the chance to meet other PhD students from both Lund and Hamburg and learn new skills.

Thanks to the beamline personnel who has helpt us during beamtimes: Ulrich Lienert, Zoltán Hegedűs, Timo Müller, Sven Gutschmidt, and Malte Blankenburg at P21.2, DESY; Olof Gutowski at P07, DESY; Ethan Crumlin at Beamline 9.3.2, ALS. You have all been most helpful and competent.

Not to forget the economic part. Thanks to the Knut and Alice Wallenberg Foundation and the Swedish Scientific Research Council for financing my PhD project. Also thanks to Patrik Wirgin, economist at the division, for help with questions regarding economy (and for being a nice dude).

There is also a bunch of other people who deserve my thanks. Jason Weaver and Vikram Mehar at the University of Florida in Gainesville, for collaboration on Pd(100) and its oxides. Jens Falta and Jon-Olaf Krisponeit at the University of Bremen, for performing LEEM on our PdAu single crystal (even though we did not get far with that experiment). Raoul Gastel at Surface Preparation Laboratory (SPL.EU), the Netherlands, for polishing our single crystals. Lindsay Merte at Malmö University, for experimental help. Mikhail Shipilin at Stockholm University, for providing me with a HESXRD plugin for ImageJ (though ImageJ mistook it for malware). Johan Zetterberg at Combustion Physics, Lund University, for internal inspection of my thesis (it was a confidence boost to read).

To my family. We all had a tough time, all these years ago. We were all affected in different ways, and I am sorry we could not help each other. I wished so many things had been different, but it turned out quite well in the end, I guess. My parents, Bo-Gunnar and Eila, you have always supported me to do my best. I know I am bad at saying it, but I love you. My sisters and their families: Anneli, Calle, Erik, Gustav, and Axel; Lisett and Niffe, I love you too.

I probably would not be where I am today without my partner, Kim. You have been my rock since we met as LTH students all these years ago. Thank you for still being a part of my life, despite all my peculiarities. I love you beyond words. I also want to thank Thomas and Kristina, the best parents-in-law I could ever wish for. And my brothers-in-law and their families: Emil, Emma, Iris, and Bodil; Johan and Sara; Viktor and Ellen; Oskar. The whole extended Svensson family! How I love to be a part of it.

To all my other friends who have not been mentioned yet. Linnea; Malin; Joakim (a.k.a. Hovslagarn); Anders; Fia; Sofie and Mikael; Sophie and Jonas. Thank you for all the boardgames, roleplaying games, our quirky injokes, all the puns (I am looking at you, Hovslagarn), and making me laugh so hard I need extra doses of my asthma medicine. I am truly lucky to have you all in my life.

To my gorgeous cat Fabian, for ”helping” me writing my thesis by reminding me to take little breaks to admire what is right in front of me (i.e. Fabian). Thank you for being beautiful and cuddly and generally... cat.

I also want to thank Gerdahallen for the possibility to work out regularly. After the pandemic break, I realised how well-being physical exercise can be for my mental health. Especially thanks to the YinYoga instructors, your classes have been excellent for my inner peace. Namaste.

I guess I should also thank Duloxetine for restoring my serotonin and norepinephrine to normal levels (no Sertraline, I am not going to thank you and you know why).

To you who broke me down when you should have built me up. You who, with a total lack of responsiveness, claimed to be right and made me feel I was not good enough, I who could not live up to your standard. If I had only known about the deep wounds you hid inside, the wounds you feared would fester in me, I would have seen you in a different light. I thought you wanted to fill me with shame, when you only tried to help me in the only way you could. We were both too young to understand, but we have both grown wiser since then. I am glad that we have sorted things out between us. You know who you are.

To ”little Helen”. It was not your fault. You could not possibly understand the long-term consequences of an unprocessed trauma. You were so young, even though you thought yourself so mature. You only tried to protect yourself by becoming hard and unfeeling. Instead you became hard and brittle. Glass instead of stone, not realising the cracks before you shattered. It is a great sorrow you did not get the help you needed, then perhaps you could have avoided what lies ahead of you. It will take many years, but soon you will understand how long the path into depression can be, how insidious this malady is. At first, you do not realise how your mood darkens, how much more difficult it becomes to concentrate and remember, how exhausted you become even from small activities. You will be tired in a way that has nothing to do with lack of sleep. The impairment of your cognitive abilities will make you question your own intelligence. When you think that your self-esteem cannot get any lower, your self-esteem just ”watch me”. You will just think it is a normal aging thing, but one day, you will wake up and realise you cannot go on like this. You will find the courage to tell the truth about your mental ailment, and you will get help. You will have to go deep into yourself to solve your problems. You will face ghosts from your past, and it will hurt, but it will be worth it. Remember, you are not alone.

To my inner demons. You told me it was futile. You told me I could just as well give up. You told me my glory days were long past. You told me I was unworthy. You told me I did not deserve self-esteem. You told me I would never be happy again. You told me no one would care. You told me I was too introvert, too incompetent, too inadequate to ever accomplish anything. You were wrong.

Popular Scientific Summary

A catalyst is a substance that enables a chemical reaction without being used up in the process. For example, a catalyst in a car engine enables the process of transforming carbon monoxide into carbon dioxide. This process has a much higher chance of happening when performed on a surface, compared to in air, as the oxygen molecule must split into atoms, which is much easier on a catalyst surface than in air. Different surfaces will affect the process differently, and understanding the structure of the surface provides insight into building better catalyst surfaces.

Even though catalysts are often utilised in the industry, there are large gaps in the knowledge about what actually happens on the surface at the atomic level when catalytic reactions occur. Catalyst development has mostly been done by trial-and-error, i.e. different combinations of materials, temperature, pressure etc. are tested for evaluation. This method takes a lot of time, and it is also very costly. Therefore, it is desirable to know what happens on the atomic scale, to better predict how useful a certain catalyst is.

One way to improve catalysts is to use alloys, i.e. mixtures of two or more metals. Alloys containing one catalytically active metal and one more inert metal often show better catalytic properties compared to the pure elements. When a metal is part of an alloy, its binding properties change, and atomic segregation can lead to surface structures that affect the catalytic function of the surface.

In this thesis, I have studied the surfaces of two alloys, namely platinum-rhodium and palladium-gold, using a technique called *surface X-ray diffraction*. High-energetic X-rays hit the atoms in the sample surface and scatter towards a detector, producing an image of the X-ray scattering. Such diffraction images can tell us what the surface structure looks like, and how it changes during the catalytic process.

We performed carbon monoxide oxidation on the platinum-rhodium sample in order to evaluate a new beamline. We chose this alloy sample because it well-studied and we knew what to expect, but hopefully we could learn something new as well. We exposed the sample to a constant flow of carbon monoxide and a varying flow of oxygen. At intermediate and high oxygen flow, we found two oxygen structures that were expected. At low oxygen flow, however, we expected a disordered surface but found a well-ordered structure resembling a checkerboard pattern. These three structures were compared with theoretical simulations of how the surface of the platinum-rhodium sample might look like at the atomic scale.

Palladium-gold samples with varying palladium-gold-ratios were oxidised as a continuation of a previous study of methane oxidation over a palladium sample. When the oxide grew too thick, the catalytic activity decreased, but when the oxide decomposed, the catalytic activity increased again. One theory is that the thick palladium oxide exposes a low-active surface

orientation, while the thin oxide exposes a high-active surface orientation. The idea behind the palladium-gold project is that the gold should limit the amount of palladium that could be oxidised, so that the oxide would remain thin enough and expose the high-active surface orientation. The results of the oxidation experiment was that we obtained a mix of different surface orientations, mostly the low-active one. However, it seems like the samples with lower gold concentration showed more of the high-active surface orientation. Therefore, it would be worth to redo the experiments with samples containing more palladium and less gold.

We also used a technique called *ambient-pressure X-ray photoelectron spectroscopy* on the thin film sample with the highest palladium-gold-ratio while oxidising the sample and then reducing the oxide with methane. This experiment supported previous studies showing that some surfaces are more catalytically active than others. We also found that the sample could be oxidised at lower oxygen pressure than we had observed in our surface X-ray diffraction study. The presence of gold in the substrate seemed to make the palladium oxide less stable.

Populärvetenskaplig Sammanfattning

En katalysator är ett ämne som möjliggör en kemisk reaktion utan att förbrukas under processen. Till exempel möjliggör en katalysator i en bilmotor processen att omvandla kolmonoxid till koldioxid. Denna process har mycket högre chans att hända när den görs på en yta jämfört med i luften, då syremolekylen måste delas i atomer, vilket är mycket lättare på en katalysatoryta än i luft. Olika ytor påverkar processen olika och förståelse av ytstrukturen ger insikt i hur man bygger bättre katalysatorytor.

Trots att katalysatorer ofta används i industrin så är det mycket som inte är känt om vad som faktiskt händer på ytan på atomnivå när katalytiska reaktioner sker. Katalysatorutvecklingen har mestadels skett genom att prova sig fram med olika kombinationer av material, temperatur, tryck etc. som testas för utvärdering. Denna metod tar mycket tid, och den är dessutom mycket kostsam. Därför är det önskvärt att veta vad som händer på atomskalan för att bättre kunna förutse hur användbar en viss katalysator är.

Ett sätt att förbättra katalysatorer är att använda legeringar, d.v.s. blandningar mellan två eller flera metaller. Legeringar som innehåller en katalytiskt aktiv metall och en mer inert metall uppvisar ofta bättre katalytiska egenskaper jämfört med de rena grundämnena. När en metall är del av en legering så ändras dess bindningsegenskaper och atomsegregering kan leda till ytstrukturer som påverkar ytans katalytiska funktion.

I den här avhandlingen har jag studerat ytorna hos två legeringar, nämligen platina-rodium och palladium-guld med en teknik som kallas *ytröntgendiffraktion*. Högenergetiska röntgenstrålar träffar atomerna i provytan och sprids mot en detektor, vilket skapar en bild av röntgenspridningen. Sådana diffraktionsbilder kan berätta för oss hur ytstrukturen ser ut och hur den förändras under den katalytiska processen.

Vi utförde kolmonoxidoxidering på platina-rodiumprovet för att utvärdera ett nytt strålrör. Vi valde detta system för att det är välstuderat och vi visste vad vi skulle vänta oss, men förhoppningsvis kunde vi lära oss något nytt också. Vi exponerade provet för ett konstant flöde av kolmonoxid och ett varierande flöde av syre. Vid måttliga och höga syreflöden fann vi två oxidstrukturer som var väntade. Vid lågt syreflöde, däremot, förväntade vi oss en oordnad yta men fann en välordnad struktur som likar ett schackmönster. Dessa tre strukturer jämfördes med teoretiska simuleringar av hur ytan på platina-rodiumprovet kunde se ut på atomnivå.

Palladium-guldprover med varierande palladium-guld-förhållanden oxiderades som en fortsättning på en tidigare studie av metanoxidering över ett palladiumprov. När oxiden växte sig för tjock så minskade den katalytiska akvtiviteten, men när oxiden bröts ner så ökade den katalytiska aktiviteten igen. En teori är att den tjocka palladiumoxiden exponerar en lågaktiv ytorientering, medan den tunna oxiden exponerar en högaktiv ytorientering. Idén

bakom palladium-guld-projektet är att guldet borde begränsa mängden palladium som kan oxideras så att oxiden skulle bli tunn nog att exponera den högaktiva ytorienteringen. Resultaten av oxideringsexperimentet var att vi fick en blandning av olika ytorienteringar, mestadels den lågaktiva. Dock verkar det som att proven med lägre guldkoncentration visade mer av den högaktiva ytorienteringen. Därför skulle det vara värt att göra om experimenten med prover som innehåller mer palladium och mindre guld.

Vi använde också en teknik som kallas *högtrycksfotoemission* på tunnfilmsprovet med det högsta palladium-guld-förhållandet medan vi oxiderade provet och sedan reducerade oxiden med metan. Detta experiment stödde tidigare studier som visat att vissa ytor är mer katalytiskt aktiva än andra. Vi fann även att provet kunde oxideras vid lägre syretryck än vi hade observerat i vår ytröntgendiffraktionsstudie. Närvaron av guld i substratet verkade göra palladiumoxiden mindre stabil.

Introduction

Why do we want to study the surfaces of catalysts? Well, for the simple reason that catalytic reactions are occurring on the surfaces of catalytic materials, and thus, the surface structure of the active phase and the gas-solid interaction are important for the desired results [1]. Also, as Kitchin et al. wrote in a paper from 2008 [2]:

> "It is difficult to understand the catalytic behavior of a surface if the actual composition and structure of that surface is unknown."

Even though catalysis is a well-known phenomenon, the details of the catalytic reaction on the atomic level are not fully understood [3]. Since the use of catalysts started, the method of developing new catalysts has mostly been the trial-and-error mode, which is both time-consuming and expensive [4, 5, 6]. Real catalysts are, however, very complex systems and difficult to study on a fundamental level. In surface science, we study model systems, which are much simpler, and we usually expose them to controlled gas flows at low pressure, while the operating conditions for real catalysts are closer to ambient conditions [3]. But if we can understand what happens at the surface on the atomic level during catalytic reactions, and find out what makes a surface high-active or low-active, we can make more educated guesses while developing new catalysts and what next step to take in catalysis research.

Catalytic alloys and bimetallic systems often have the advantage of being better catalysts compared to their pure components [7, 8]. The surface composition of an alloy or a bimetallic system differs from the bulk composition, and there is often strain in the crystal lattice due to varying sizes of the atoms [9]. Alloys are also advantageous for studying the segregation of different atoms [10]. When two or more metals are alloyed, the chemical and physical properties of the metallic constituents are changed [11].

In this thesis, I have investigated the surfaces of model alloy catalysts in the shape of single crystals and thin film samples. I have studied the surfaces under reaction conditions with mainly SXRD, and also some APXPS. It started with pure Pd, as I studied how the low-

active PdO(100) [3] forms on a Pd(100) single crystal (Paper III), to later continue with bimetallic systems such as PtRh (Paper I and Paper II) and PdAu (Paper IV and Paper V).

The PtRh system described in Paper I and Paper II is a $Pt_{25}Rh_{75}(100)$ single crystal studied at the Swedish Materials Science Beamline (P21.2) [12] at PETRA III, DESY in Hamburg, Germany. It was a commissioning beamtime (i.e. a beamtime for testing a new beamline) and the bimetallic crystal was studied with HESXRD under reaction conditions, and the model reaction was CO oxidation, due to its simplicity [13]. The PtRh system was chosen because it is well-studied [7, 14, 15, 16, 17, 18, 19, 20, 21, 22, 23] and we knew what to expect, but we also believed we might find something new (which we did, more about that in Paper I and Paper II).

Most experiments in Paper III were done at the University of Florida, Gainesville in Florida, USA (LEED and TPD) and at the High-Energy Beamline for Buried Interface Structure and Materials Processing (ID31) [24] at ESRF in Grenoble, France (TSD) before I started my PhD. However, I have worked with the analysis of the diffraction data.

The oxidation experiments on PdAu thin film samples – performed at P21.2 – described in Paper IV build on a study by Hellman et al. from 2012 [4], where they investigated which was the active Pd phase during methane oxidation. They found that when the PdO film thickness increased, the catalytic activity increased up to a certain point and then started decreasing even as the oxide film continued to grow and the temperature increased. When the oxide was decomposed, the catalytic activity increased again. By exchanging Pd for PdAu, the idea was to limit the amount of Pd that can be oxidised and thus keep the PdO film thin enough to stay active. Furthermore, PdAu has shown less sensitivity to oxygen poisoning [25, 26]. The APXPS experiments on the PdAu thin film samples in Paper V were performed at the Ambient-Pressure Soft X-ray Photoelectron Spectroscopy (Beamline 9.3.2) [27, 28, 29] at ALS (Advanced Light Source) in Berkeley, San Francisco in California, USA.

This thesis will contribute to increased understanding of the physics and chemistry of surfaces and how they relate to catalysis, as well as discussing alloys in a catalytic context. The methods that have been used in my PhD project – either by me or by some of my colleagues – will be described. Finally, the papers included in this thesis will be summarised, and I will discuss my results and insights gathered during my PhD, as well as draw conclusions and speculate about the future.

Surface Science and Catalysis

When investigating surfaces and interfaces at the atomic level, a lot of interesting phenomena can be observed. The study of such phenomena, which may be of physical or chemical nature, is called *surface science*. [30] Many different research areas are included in surface science, and one of them is *catalysis*, the promoting effect some substances (called *catalysts*) have on certain chemical reactions [31]. Catalytic reactions occur on surfaces, but not any surfaces. The structure of the catalyst surface is important for its catalytic function. The physics and chemistry of the surface dictate whether reactants are able to adsorb and react with each other, and if the product can desorb from the surface. This chapter will describe the basics of how crystalline materials are built up and how superstructures are denoted, as well as how catalysis works. Finally, the alloy systems studied in this thesis, PtRh and PdAu, will be described in a catalytic context.

Unit Cells, Planes, and Lattices

The structure of a crystalline material can be described as a periodic lattice where the atoms sit in the lattice points, the so-called *Bravias lattice*[1]. The smallest unit of a lattice is called a *unit cell*, defined in a way that if several unit cells are concatenated, they form the *crystal lattice*. Thus, the lattice repeats itself. The unit cell can have different shapes, such as cubic, tetragonal, hexagonal, orthorhombic, rhombohedral, monoclinic, and triclinic. [32]

Figure 1 shows a cubic unit cell, where the side-lengths are denoted *a*, *b*, and *c*. The angles are denoted α (between *b* and *c*), β (between *a* and *c*), and γ (between *a* and *b*). Since the unit cell is cubic, all sides are equal, i.e. $a = b = c = a_0$, and all angles are orthogonal, i.e. $\alpha = \beta = \gamma = 90°$. Here, a_0 is called the *lattice constant*. [32]

The simplest unit cell is called *simple cubic* (SC), see Figure 2a. It has one atom in each lattice point. If one atom is added in the center of the unit cell, a *body centered cubic* (BCC) is obtained, see Figure 2b. Adding one atom to each face of the SC unit cell gives a

[1]Named after the French physicist Auguste Bravais $(1811 - 1863)$.

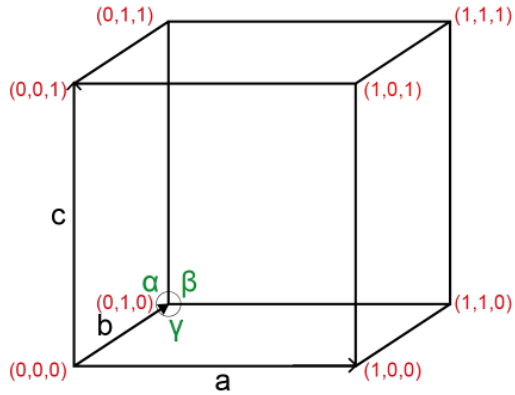

Figure 1: The sides in the unit cell are denoted *a*, *b*, and *c*. The angles (green) are denoted α, β, and γ. *Recreation of Figures* 3-6 *and* 3-11 *in [32].*

face centered cubic (FCC), see Figure 2c. [32] Many metals, including Pd, Pt, Rh, and Au, which are studied in this thesis, are FCC [31].

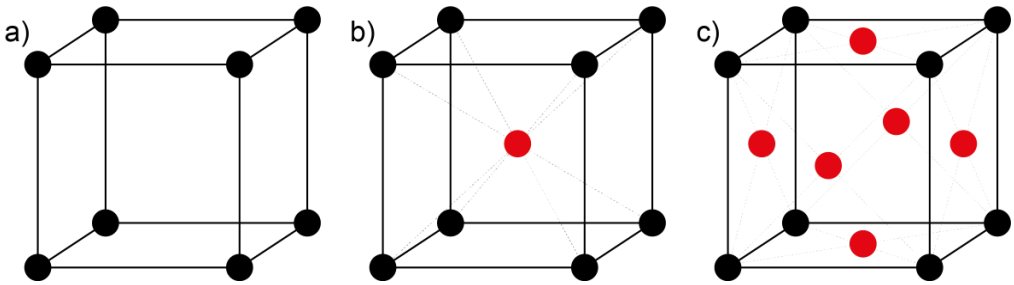

Figure 2: There are different types of unit cells. The most common ones are the simple cubic (SC) unit cell (a), the body centered cubic (BCC) unit cell (b), and the face centered cubic (FCC) unit cell (c). The black discs indicate the SC unit cell and the red discs indicate the atoms that need to be added to get the BCC and FCC unit cells, respectively. *Recreation of Figure* 3-5 *in [32].*

Any two points in the Bravais lattice are connected by the vector **R**, see Equation 1. One can describe the whole crystal by translating **R**.

$$\mathbf{R} = n_1\mathbf{a} + n_2\mathbf{b} + n_3\mathbf{c}, \quad n_1, n_2, n_3 \in Z \tag{1}$$

To create a surface, a crystal is cut along a certain plane. The orientation of this plane is given by the so-called *Miller indices*[2], which are found by the reciprocals of the intercepts of the plane with the *a*, *b*, and *c* axes, see Figure 3. To decide what plane the crystal is cut along, one has to take the reciprocals of the intercepts at the *a*, *b*, and *c* axes. In case

[2]Named after the Welsh mineralogist William Hallowes Miller (1801 – 1880).

the plane does not intercept an axis, it is said to intercept the axis in infinity (thus, the reciprocal is 0). In Figure 3a, the intercepts are $(1, \infty, \infty)$ and thus the Miller indices of this plane are (100). The same method gives Miller indices of (110) in Figure 3b and (111) in Figure 3c. [33] The atoms in the surface are described by a 2D surface lattice given by

$$\mathbf{R}_s = n_1\mathbf{a}_s + n_2\mathbf{b}_s, \quad n_1, n_2 \in Z \tag{2}$$

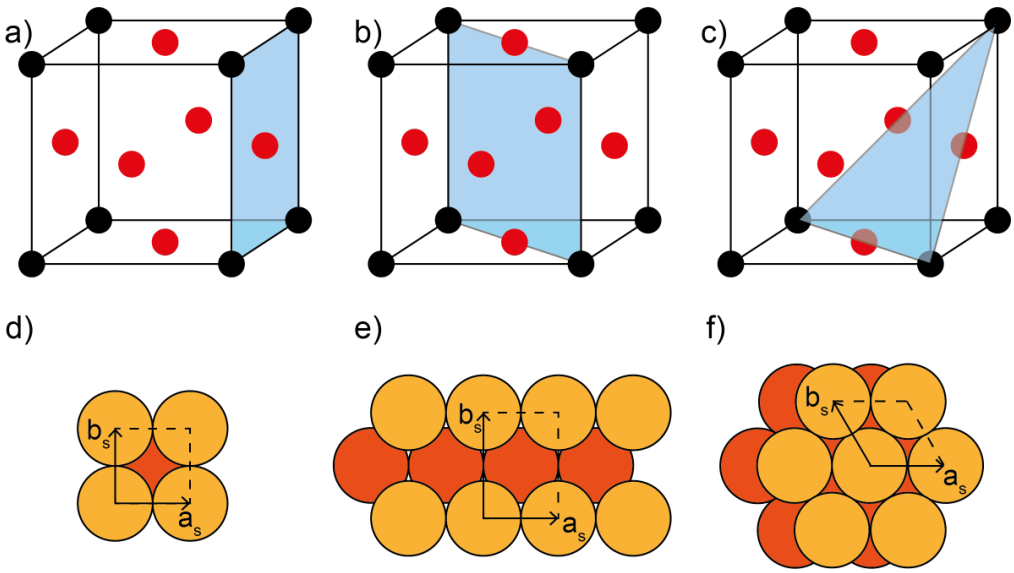

Figure 3: Three different planes (light blue) are shown here in the FCC unit cell (a-c), as well as the 2D projections (black dashed parallelograms), where the different colours indicate different layers (d-f). The planes are the (100) plane (a,d), the (110) plane (b,e), and the (111) plane (c,f). *Recreation of Figures* $1.14 - 1.15$ *in [33].*

Depending on the orientation of the surface plane, the surface atoms will have different arrangements. This will, for instance, affect how close the atoms are to each other, which will in turn affect their reactivity. The (100) surface is more open than the (111), and consequently, O_2 adsorbs more easily on Pd(100) than on Pd(111) [34]. If the surface has the same orientation as the bulk, the crystal is said to be *bulk terminated*.

Superstructures

The periodicity at the surface is often different as compared to the bulk termination. This can be the result of changes in atomic bonds, when the crystal is cut, or caused by adsorption

of other molecules. Such an overlayer structure, also known as a *superstructure*, is most often described by *Wood's notation*[3] [35]. Wood's notation is given by

$$\mathrm{N}\left(\frac{|\mathbf{a}_\mathrm{o}|}{|\mathbf{a}_\mathrm{s}|} \times \frac{|\mathbf{b}_\mathrm{o}|}{|\mathbf{b}_\mathrm{s}|}\right)\mathrm{R}\Theta \tag{3}$$

where N denotes the type of structure (i.e. p for *primitive* (often omitted) and c for *centered*), $|\mathbf{a}_\mathrm{o}|$ and $|\mathbf{b}_\mathrm{o}|$ are the magnitudes of the overlayer net vectors, $|\mathbf{a}_\mathrm{s}|$ and $|\mathbf{b}_\mathrm{s}|$ are the magnitudes of the substrate net vectors, and Θ is the angle of rotation ($\mathrm{R}\Theta$ is omitted if $\Theta = 0°$). [33]

In Figure 4, a clean surface (Figure 4a) and a surface with a superstructure (Figure 4b) are shown. This specific superstructure can be denoted either $\mathrm{c}(2 \times 2)$ or $(\sqrt{2} \times \sqrt{2})\mathrm{R}45°$.

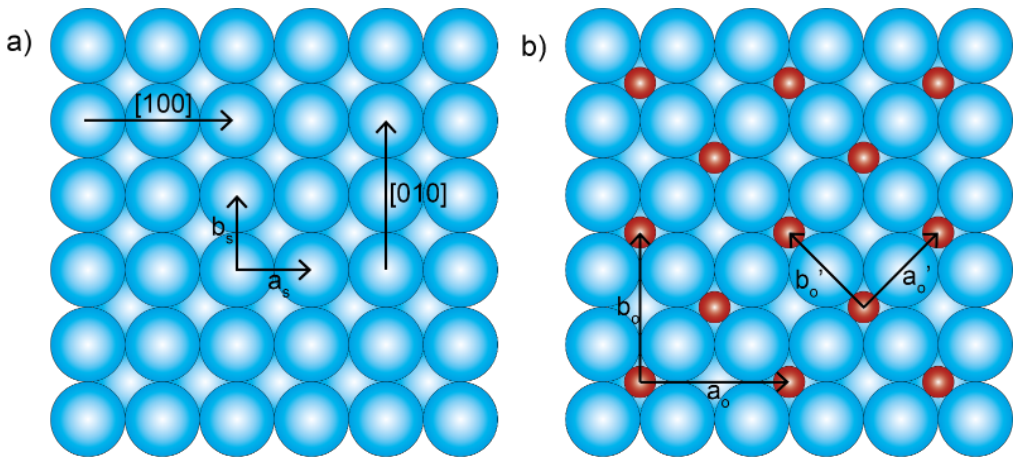

Figure 4: Clean FCC(100) surface with (1×1) structure (a) and c(2×2) superstructure (b). This superstructure is the same as $(\sqrt{2} \times \sqrt{2})\mathrm{R}45°$. *Recreation of Figure* 1.35 *in [33].*

Samples

Single Crystals

A *single crystal* is a bulk crystal with unbroken periodicity, giving it a surface of one single orientation. However, single crystals are usually not perfect; they often contain lots of small domains of different orientations (to calculate their average size, see Equation 31). The crystal we investigated in Paper I and Paper II was a PtRh single crystal with the surface orientation (100) and a Pt:Rh ratio of 1:3.

[3]Named after the American crystallographer and geologist Elizabeth Armstrong Wood $(1912 - 2006)$.

Thin Film Samples

Figure 5 shows a schematic drawing of the thin film samples we investigated in Paper IV and Paper V. Thin metallic films of Pd and Au were deposited onto the substrate by electron-beam physical vapour deposition (EBPVD).

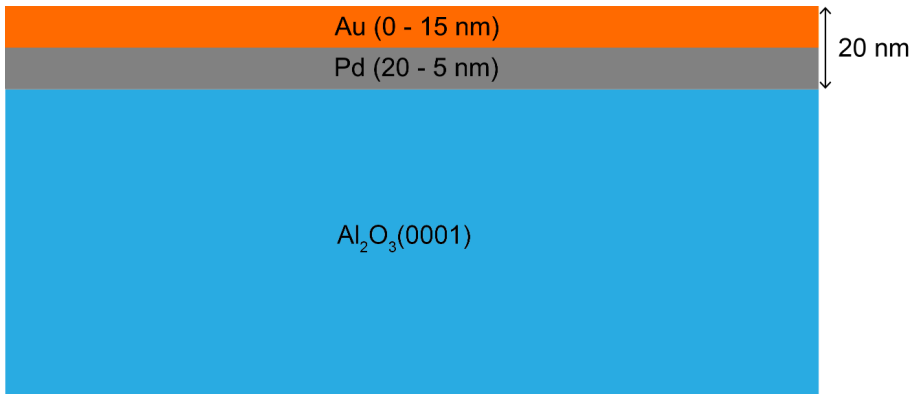

Figure 5: Schematic drawing of our PdAu thin film samples. Thin films of Pd and Au where deposited on a sapphire substrate. Note that the film and substrate thicknesses are not made to scale.

As can be seen in the figure above, the thickness of the Pd and Au films varied, but the total metallic film was (in most cases) 20 nm. We used samples with the following Pd:Au ratios: 20:0, 15:5, 10:10, 5:15, and 5:5 (note that this sample had a total metallic film thickness of 10 nm instead of 20 nm). We also tried reversing the deposition order, having Pd on top (Pd:Au = 10:10). Figure 5 shows the Pd and Au metals as separated films, which is the state of the pristine (as prepared) samples. Thus, we started with a bimetallic system which became an alloy after annealing. Our method of investigating the alloying and oxide formation was GIXRD, at the same beamline as the PtRh experiments. The results of oxidising PdAu thin film samples can be read in Paper IV, and the APXPS results in Paper V.

Adsorption, Desorption, and Oxide Formation

For a catalytic reaction to occur, the bonding strength between the reactants and the catalyst and between the product and the catalyst must be neither too weak nor too strong in order to have a reaction. Consider a reaction where reactants A and B form product AB. If the reactant-catalyst bond is too weak, the reactants will desorb before any reaction can take place. If the bond between A and the catalyst is too strong, on the other hand, the active sites will be occupied with A so that B cannot adsorb to react with A. This is called *poisoning*,

and the catalyst could also become poisoned by the product, AB, if its bond to the catalyst is too strong. [31] This is called *Sabatier's principle*[4].

Often, there are specific so-called *active sites* on the catalyst, where the catalytic reaction occurs, and the structure, chemical properties, and distribution of these sites determine the catalytic activity [2]. These are often so-called *coordinatively unsaturated* (CUS) sites, which, due to their dangling bonds, are more reactive and can more easily adsorb and dissociate the reactants. On metal surfaces, these can for instance be at steps or kinks. In an alloy, these sites can also be affected by neighbouring atoms of a different metal. In an oxide, there might be CUS metal atoms at the surface. These all depend on the atomic structure of the catalyst surface. [3, 36, 37, 38, 39, 40, 41, 42, 43]

There are mainly two types of adsorption: physisorption and chemisorption. The difference lies in the bonding interaction. In physisoption, the adsorbate bonds weakly to the substrate and interacts through long range van der Waals forces[5]. In chemisorption, there is an exchange of electrons between the adsorbate and the substrate. [33]

When a gas molecule adsorbs on the surface of the substrate, it can do so with or without fragmentation. The former is called *dissociative adsorption*, e.g. when an O_2 molecule adsorbs and breaks into two O atoms. The latter is called *associative adsorption*, e.g. when a CO molecule adsorbs and stays intact.

When an atom or a molecule adsorbs on a substrate, there are different sites where it can adsorb, see Figure 6. On a (100) surface, it can adsorb on top of a substrate atom (*atop site*), in the hollow between four substrate atoms (*four-fold hollow site*), or it can form a bridge between two substrate atoms (*bridge site*), see Figure 6a. On a (110) surface, atop sites and bridge sites are possible, see Figure 6b. On a (111) surface, the adsorbate can adsorb on an atop site, a bridge site, or a *three-fold hollow site*, either FCC or HCP, see Figure 6c. [44]

When adsorbed oxygen does not stay at the surface, but mixes with the metal to form a new compound, we call this compound an *oxide*. During the oxide formation, the oxygen atoms have to penetrate the surface and the atoms are rearranged. Hence, this requires a significant amount of mobility and typically occurs only at elevated temperatures. It also occurs easier on open surfaces or at steps, where the metal atoms do not need to be displaced as much to allow for O to penetrate. [45]

[4]Named after the French chemist Paul Sabatier (1854 – 1941).

[5]Named after the Dutch theoretical physicist and thermodynamicist Johannes Diderik van der Waals (1837 – 1923).

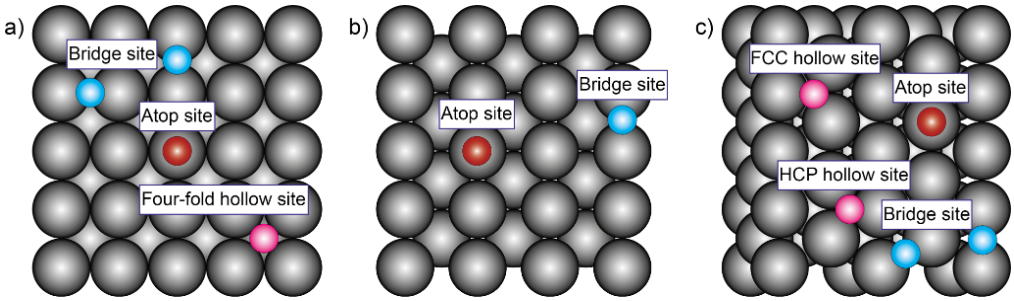

Figure 6: An adsorbate can adsorb on different sites. On (100) surfaces, it can adsorb on bridge sites, atop sites, and four-fold hollow sites (a). On (110) surfaces, it can adsorb on bridge sites and atop sites (b). On (111) surfaces, it can adsorb on bridge sites, atop sites, and three-fold hollow sites (FCC and HCP) (c). Colours: black – substrate, cyan – adatoms on bridge sites, red – adatoms on atop sites, magenta – adatoms on hollow sites. *Recreation of Figure* 5.6 *in [31].*

Reaction Mechanisms

Heterogeneous catalysis can occur through different reaction mechanisms [31]. Three common mechanisms will be described below. The *Langmuir-Hinshelwood mechanism*[6] (LH) [46, 47] occurs when two reactants, A and B, both adsorb on the catalyst surface, react with each other in adsorbed state, and finally the product, A-B, desorbs back to gas-phase. The *Eley-Rideal mechanism*[7] (ER) [48] resembles the LH mechanism, with the difference that only reactant A adsorbs while reactant B remains in the gas-phase. After reaction, A-B desorbs form the surface. The *Mars-van Krevelen mechanism*[8] (MvK) [49] requires a metal oxide to occur. The reactant in the gas-phase adsorbs on an O atom in the oxide and the oxidised product then desorbs, leaving a vacancy in the oxide. Then, O from the gas-phase fills the vacancy.

Carbon Monoxide Oxidation

In heterogeneous catalysis, the CO oxidation reaction,

$$2CO + O_2 \rightarrow 2CO_2 \tag{4}$$

is one of the most studied reactions [50]. It is often used as a model system for oxidation

[6]Named after the American chemist, physicist, and engineer Irving Langmuir (1881 – 1957) and the British physical chemist Cyril Norman Hinshelwood (1897 – 1967).

[7]Named after the chemist Daniel Douglas Eley (1914 – 2015) and the physical chemist Eric Keightley Rideal (1890 – 1974), both British.

[8]Named after the scientist Pieter Mars (1921 – 2009) and the chemical engineer and coal and polymer scientist Dirk Willem van Krevelen (1914 – 2001), both Dutch.

catalysis due to its simplicity; the only product that can be formed is CO_2, and the rate-determining step (RDS) is the dissociation of O_2 (which is spontaneous upon adsorption [3, 51]). However, if the catalyst surface is CO poisoned, as it often is at low temperature, the RDS is rather the desorption of CO in order to make place for O_2 adsorption. [13] CO oxidation is also directly relevant to industry, which also leads to many studies of CO oxidation [51].

On a metallic surface, CO oxidation proceeds through the LH mechanism. Figure 7 shows this reaction mechanism over PdAu. Starting in gas-phase (a), both CO and O_2 adsorb on the Pd atoms (b), and the latter needs to dissociate into atomic O (which happens spontaneously as the O_2 molecule adsorbs [3, 51]) to enable the reaction (c). After reaction (d), the CO_2 molecules desorb back to gas-phase (e).

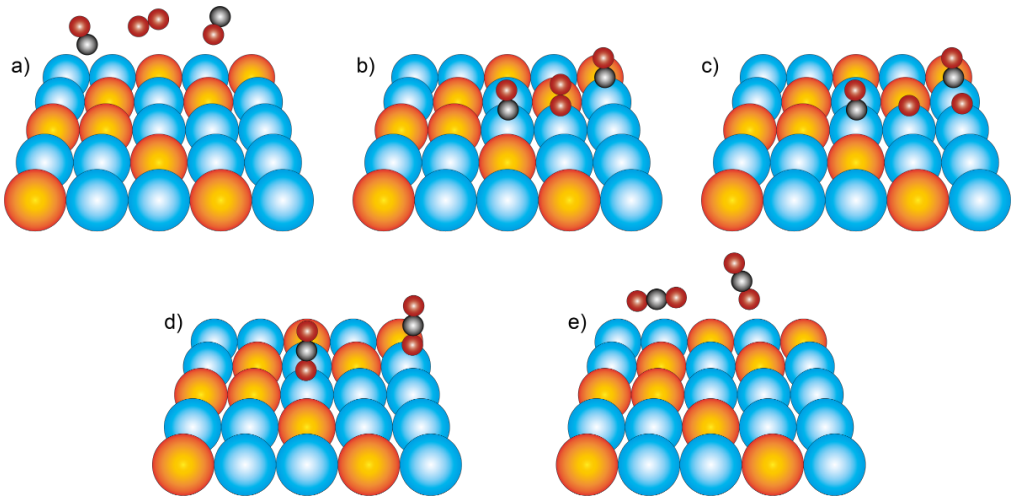

Figure 7: The CO oxidation often proceeds through the LH mechanism. CO and O_2 in the gas-phase (a) adsorb on the surface of the catalyst (b). Then O_2 dissociates into atomic O (c), which reacts with CO to form CO_2 (d). Finally, CO_2 desorbs from the surface (e). For each O_2 molecule, two CO molecules are required to form two CO_2 molecules, see Equation 4. Colours: red – O, black – C, cyan – Pd, flame-coloured – Au.

If CO oxidation takes place on the surface of an oxide, the reaction mechanism will be MvK. An example of this can be seen in Figure 10d, where CO and O_2 form CO_2 over a thin PdO film.

The major energy barrier is the O_2 dissociation, e.g. the splitting of this molecule into two O atoms [3]. In the O_2 molecule, the two O atoms are attached to each other with a double bond, and the bond dissociation energy is 498 kJ[9]/mol [52]. This energy barrier is removed by the catalyst, since it requires much lower energy to dissociate the O_2 molecule on the catalyst surface.

[9]Named after the English physicist and mathematician James Prescott Joule (1818 – 1889).

Methane Oxidation

Another oxidation process is that of methane. It can be completely oxidised (Equation 5), e.g. on Pd, or partially oxidised (Equation 6), e.g. on Pt [53]. The assumed RSD of methane oxidation is the dissociation of the first H atom [4, 36].

$$\text{Complete oxidation: } CH_4 + 2O_2 \rightarrow CO_2 + 2H_2O \tag{5}$$

$$\text{Partial oxidation: } 2CH_4 + O_2 \rightarrow 2CO + 4H_2 \tag{6}$$

Compared to CO_2, methane has shorter longevity but higher heat trapping capacity. This makes the time-frame important. Say that we release the same amounts of CO_2 and methane today and compare their heat trapping capacities in 20 years and again in 100 years. In the shorter time-frame, methane shows $84 - 86$ times as high potency as CO_2, but in the longer time-frame, methane is "only" $28 - 34$ times as potent as CO_2. [54]

Catalysis

A catalyst is a substance that alters the reaction rate of a chemical reaction without being consumed. The word *catalysis* is derived from the Greek words *kata* (down) and *lyein* (loosen), and it was coined in 1835 by the Swedish chemist Jöns Jakob Berzelius ($1779 - 1848$). He defined catalysis as [55]:

> "The property of exerting on other bodies an action which is very different from chemical affinity. By means of this action, they produce decomposition in bodies, and form new compounds into the composition of which they do not enter".

Some decades later, the Baltic German chemist and philosopher Friedrich Wilhelm Ostwald ($1853 - 1932$) studied a number of chemical reactions, some with an acid or a base present, to find out the reaction speed. He provided an explanation in 1894 which lead to the Nobel Prize[10] in Chemistry 15 years later: the speed of a chemical reaction can be increased by a substance that is excluded from the end-products, and such a substance is called a *catalyst*. Thus, Berzelius gave name to the action – *catalysis* – and Ostwald gave name to the substance

[10] Named after the Swedish chemist, engineer, inventor, businessman, and philanthropist Alfred Bernhard Nobel ($1833 - 1896$).

causing this action – *catalyst*. However, the phenomenon of catalysis has been known since long before the 19th century, although the understanding of this phenomenon was born at this time. [55]

Nowadays, catalysts are important components in the chemical industry, for instance in oil refineries, pollution prevention, and production of bulk and fine chemicals. As much as $85 - 90\%$ of the chemical industry products are manufactured via catalytic processes. What the catalyst does is to offer an energetically more favourable route for the reaction to occur, see Figure 8. It changes the kinetics, but the thermodynamics remain unchanged. Thus, if the reaction is thermodynamically unfavourable, no catalyst will help. [31]

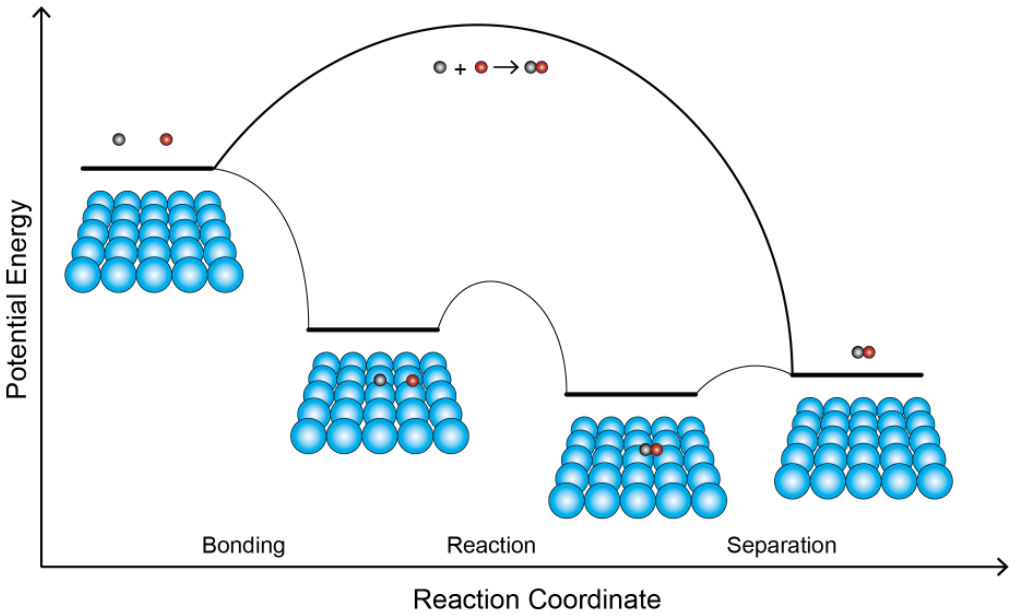

Figure 8: Potential energy diagram of heterogeneous catalysis. The catalyst lowers the energy barrier that the reaction has to overcome, and thereby provides an easier route for the reaction to occur. Colours: black – first reactant, red – second reactant, cyan – catalyst (often a transition metal). *Recreation of Figure* 1.2 *in [31].*

If the reactants and the catalyst are in different phases, the process is called *heterogeneous catalysis*. Most commonly, the catalyst is a solid and the reactants are in the gas-phase. The opposite is called *homogeneous catalysis*, i.e. the reactants and the catalyst are in the same phase (gaseous or liquid). [31] Only heterogeneous catalysis will be considered in this thesis.

Model Catalysts

The model catalysts used for experimental investigations are quite different from real catalysts used in, for instance, an automotive engine. A model catalyst usually consists of a single crystal, i.e. a crystal with only one domain. Industrial heterogeneous catalysts, on the other hand, are more complex [3]. For instance, the catalytic converter used in an automotive engine is usually built up by a honeycomb monolith in a container of stainless steel. The monolith can be ceramic or metallic and has a high cell density in order to obtain a high surface area for the washcoat, a porous alumina layer with added ceria and zirconia mixed oxides to promote the oxygen storage capacity. Nanoparticles of noble metals are dispersed on the washcoat, usually Pt and Rh, and sometimes Pd. [31] Furthermore, an element that exhibits catalytic behaviour in certain conditions does not necessarily show the same behaviour if the conditions change. One example of this is Ru, which works very well as a catalyst at high pressures, while its catalytic abilities are not particularly good under UHV compatible conditions [51].

There are mainly two gaps between catalysis and traditional surface science [56]:

- **The materials gap** – Model catalysts are usually well-ordered single crystals while real catalysts consist of nanoparticles embedded in a washcoated support. Thus, real catalysts are more complex than single crystals.
- **The pressure gap** – Experiments are usually conducted under UHV or controlled gas flows while real catalysis occurs under ambient conditions.

These gaps are wished to be over-bridged, in order to obtain a better conformity between what we see during experiments and the real world.

Alloys and Bimetallic Systems in Catalysis

Mixing at least two chemical elements, of which at least one is a metal, results in an *alloy*. If the metals are separated, it is usually called a *bimetallic system*. [11] Heating a bimetallic sample will increase the mobility of the atoms, which leads to mixing and alloy formation. Alloy catalysts are often better than pure-metal catalysts due to the fact that the chemical properties of the atoms are changed by the different surrounding compared to pure metals [2, 7, 8]. The more inert metal atoms segregate to the surface in vacuum and the most reactive metal atoms are pulled towards the surface in gas, giving the alloy a surface composition different from its bulk composition [9]. Beneath the surface of the alloy, atoms may segregate to form ordered structures, affecting the properties of the surface atoms (see

Paper II). Working with alloys, it is good to remember Vegard's law[11], which says that the lattice constant of an alloy is a linear combination of the lattice constants of its constituents [57].

The reason the surface of the alloy has another composition than its bulk is that atoms segregate. In general, bulk termination is not the most favourable configuration from an energetic perspective, so atoms from the bulk will segregate to the surface if this can lower the surface energy. [2]

Looking at the atomic scale, there are three primary mechanisms affecting the catalytic properties of the alloy surface. These mechanisms are illustrated in Figure 9. *Strain effects* occur due to changes in the lattice constant of the alloy. Depending on the concentrations of the different constituents, the alloy will have a lattice constant somewhere between those of the pure metals. This may result in a change in which surface orientations that will be stabilised. *Ensemble effects* refer to the presence of multifunctional adsorption sites that enables simultaneous bonding to different metals. *Ligand effects* are caused by the hetero-metallic bond formation occurring in alloys. The bond strength may be different for A-B than for A-A, causing the bond strength between A and an adsorbate to change. Furthermore, coverage effects may also affect the catalytic function of the alloy surface, since the active sites may be occupied so that other adsorbates cannot bond to the catalyst surface. All these effects are not independent; the changes in catalytic properties are the results of different effects coexisting and affecting each other, and it might be difficult to distinguish which changes are due to which effects. [2]

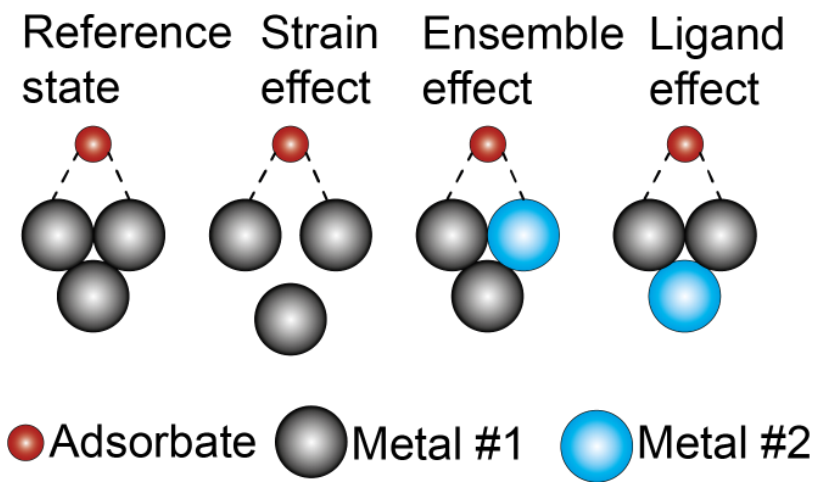

Figure 9: There are mainly three mechanisms that affect the catalytic properties of alloys: strain, ensembles, and ligands. *Recreation of Figure 2 in [2].*

[11]Named after the Norwegian physicist Lars Vegard (1880 – 1963).

Systems in This Thesis

Alloys may be more difficult to oxidise compared to their pure metal components. This has been seen for e.g. $Pt_{25}Rh_{75}(100)$ [58], a sample we have worked with too (Paper I and Paper II). Our studies on PdAu (Paper IV) also showed that this bimetallic system is significantly more difficult to oxidise than pure Pd. In Table 1, the metals constituting "our" bimetallic systems are compiled, together with some useful data.

Table 1: The elements constituting the alloys I have studied in this thesis: PtRh and PdAu. Their atomic number (Z), atomic radii, lattice constants, crystal structure, and surface energies at room temperature are given.

Element (Z) [31]	**Atomic radius** (Å) (**empirical** [59]/**calculated** [60])	**Lattice constants** (Å) [31] (**crystal structure**) [44]	**Surface energy** at **298** K (J/m^2) [61]
Rhodium (45)	1.35/1.73	3.80 (FCC)	2.828
Palladium (46)	1.40/1.69	3.89 (FCC)	2.043
Platinum (78)	1.35/1.77	3.92 (FCC)	2.691
Gold (79)	1.35/1.74	4.08 (FCC)	1.626

Looking at this table, we see that Pt and Rh have almost the same radius. These metals also have the same electronegativity, 2.28 [62], so they are likely to form an alloy. With the $Pt_{25}Rh_{75}(100)$ single crystal that we investigated in Paper I and Paper II, the lattice constant of the alloy would be 3.83 Å[12] according to Vegard's law [58, 63]. The electronegativitiy of Pd is 2.2, while this value is 2.54 for Au [62]. Their radii are also similar (see Table 1). The size difference is not so large, so these metals can alloy with each other. Thus, both PtRh and PdAu can form alloys if they are heated at sufficiently high temperature to cause atom migration. In the next sections, I will explain the natures of PtRh and PdAu, and what types of studies I have done on them.

Platinum-Rhodium

Pt and Rh are the main components in the catalytic nanoparticles used in automotive engine catalysts [7, 14, 18, 19, 20, 31, 34, 64], and as a bimetallic system, PtRh is extensively studied [7, 14, 15, 16, 17, 18, 19, 20, 21, 22, 23, 58, 63, 65]. We studied CO oxidation over a $Pt_{25}Rh_{75}(100)$ single crystal using HESXRD during a commissioning beamtime at the Swedish Materials Science Beamline (P21.2) [12] at PETRA III, DESY in Hamburg, Germany. The purpose of a commissioning beamtime is to test a new beamline, and thus, we wanted to study a sample where we knew what to expect, but still might learn something new.

In vacuum, the Pt atoms in the PtRh bimetallic system will segregate towards the surface

[12]Named after the Swedish physicist and astronomer Anders Jonas Ångström (1814 – 1874).

[14, 20, 21, 23] due to lower surface energy compared to Rh (see Table 1). Exposure to O_2, on the other hand, tends to cause Rh segregation towards the surface [21, 58], and similar oxygen structures may form as on pure Rh surfaces. Two oxygen structures that have been observed on both Rh(100) and PtRh(100) in several studies are a (3×1) reconstruction with chemisorbed O under mildly oxidising conditions [16, 19, 58, 65, 66, 67] and a $c(8 \times 2)$ surface oxide under strongly oxidising conditions [15, 51, 58, 66]. Rh is more reactive than Pt, so O rather bonds to the former than the latter [63]. Due to changed chemical and physical properties of the atoms in a bimetallic surface compared to a pure-element surface, CO adsorption on PtRh(100) is not the same as on Pt(100) or Rh(100). The surface composition affects the CO adsorption sites. For instance, if there is a Pt overlayer on a Rh substrate, the CO adsorption will be weaker due to the ligand effect (see the rightmost part of Figure 9). [14]

Pure Palladium and Palladium-Gold

Whether it is the metallic phase of Pd or its oxide phase that is the active one during the oxidation of CO and hydrocarbons (e.g. methane) has been debated [3, 34, 68]. However, it has been shown that a single PdO layer is high-active for CO oxidation and low-active for methane oxidation (Figure 10a-b), while a few layers of PdO make the surface high-active for both CO oxidation and methane oxidation (Figure 10c-d). A thick PdO film is low-active for both of them (Figure 10e-f) [3, 4, 37]. A possible explanation is that when the PdO film grows thick enough, it loses registry with the substrate and exposes the (100) facet instead of the (101) facet. PdO(101) has CUS Pd sites – i.e. Pd atoms with a dangling bond that is free to adsorbates – where the reactants can adsorb, whereas PdO(100) is saturated and has no CUS sites [3]. One theoretical study [69] says that the PdO(100)-PdO termination has very low surface energy, making it a stable PdO phase. This could explain the exposure of the (100) surface on thick PdO films. However, another theoretical study [70] says that PdO(101) on Pd(100) is the most stable orientation at any film thickness. You can read more about the formation of epitaxial PdO(100) during oxidation of Pd(100) in Paper III. In 2012, Hellman et al. [4] studied methane oxidation over a Pd(100) single crystal and found that the CO_2 production at first increased with the growing oxide film, but then started to decrease as the oxide continued to grow. When the oxide decomposed, the CO_2 production increased again. This work is the foundation for our experiments with PdAu described in Paper IV and Paper V. If we can stop the oxide growth at a suitable thickness, we could – at least in theory – keep the oxide film thin enough to expose the (101) surface and remain catalytically active for CO oxidation and methane oxidation. The idea is to alloy Pd with Au in order to create an obstructive Au top layer that makes it more difficult for Pd atoms to segregate to the surface and be oxidised. Thus we could limit the amount of Pd that can be oxidised and get an oxide film thin enough to expose the (101) surface (Figure 10g-h).

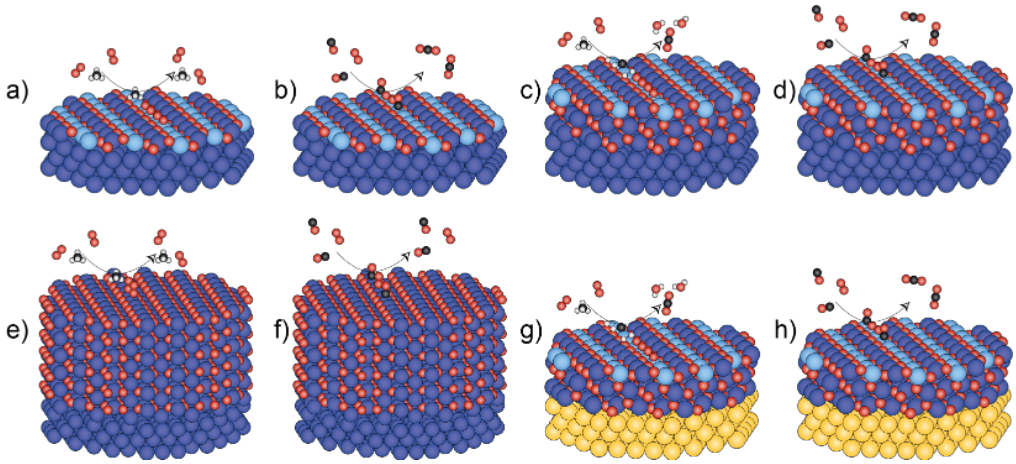

Figure 10: A single PdO layer is inactive for methane oxidation (a) but active for CO oxidation (b). If the PdO film grows to a few layers, it becomes active for both methane oxidation (c) and CO oxidation (d). If the PdO film grows too thick, however, it becomes inactive for both methane oxidation (e) and CO oxidation (f). A PdO film grown on Au could limit the thickness and keep the oxide catalytically active for both methane oxidation (g) and CO oxidation (h). Colours: blue – saturated Pd, cyan – unsaturated Pd, red – O, black – C, off white – H, yellow – Au. *Reconstruction of Figure* 4 *in [3] and Figure* 1 *in Paper* IV.

Au is more inert than Pd and has lower surface energy (as seen in Table 1), meaning it will segregate towards the surface in vacuum [71]. Exposure to a reactive gas, such as O_2 or CO, causes the more reactive Pd to segregate towards the surface [72].

Experimental Methods

In this chapter, the different experimental methods that have been used for this thesis will be described. I have not done all of them myself, but they have all been utilised for the papers included (I will be clear on which these techniques are as they are described). Since my main experimental technique has been SXRD, the emphasis will be on this technique.

Surface X-Ray Diffraction

My main experimental method has been *surface X-ray diffraction* (SXRD), to which I also include *grazing incidence X-ray diffraction* (GIXRD). This surface-sensitive technique is commonly used to provide information about the surface structure of many different types of samples, for instance single crystals, nanoparticles, and thin film samples. Before we go into the details of the instrumentation, we will take a closer look at the nature of X-rays and how they diffract.

X-Ray Diffraction

In 1895, the German physicist Wilhelm Conrad Röntgen (1845 – 1923) discovered X-rays, which had the power to penetrate matter and provide its internal structures. This ionising electromagnetic radiation has an energy in the range of 100 eV[13] to 100 keV. The X-ray energy, E, is given by

$$\mathrm{E} = \frac{\mathrm{hc}}{\lambda} \tag{7}$$

where h is Planck's constant[14], c is the speed of light in vacuum, and λ is the wavelength of

[13]Named after the Italian physicist and chemist Alessandro Volta (1745 – 1827).
[14]Named after the German physicist Max Planck (1858 – 1947).

the X-rays. Thus, the X-ray energy range corresponds to wavelengths in the range of 10 nm down to 0.01 nm, which makes it useful for studying atoms. The size of an atom is about 1 Å, i.e. in the same order of magnitude as X-rays. [73] This discovery rendered Röntgen the first Nobel Prize in Physics six years after this discovery [74].

X-rays have a wavelength on the same magnitude as the atomic spacing in the crystal. When the rays hit the atoms in the sample, they scatter in all directions. Most of the radiation is cancelled out due to destructive interference. If the X-rays scattered by different atoms are in phase, however, they interfere constructively and beams of high intensity are seen. This is called *diffraction* and happens in crystalline materials, when the X-rays hit the crystallographic planes at certain angles. [32]

The fact that crystals diffract X-rays was discovered by the German physicist Max von Laue $(1879-1960)$, a discovery that gave him the Nobel Prize in Physics in 1914. The year after, this prize went to the English physicist, chemist, and mathematician William Henry Bragg $(1862-1942)$ and his son, the physicist and X-ray crystallographer William Lawrence Bragg $(1890-1971)$, for their contribution to X-ray diffraction. [32]

Diffraction occurs in the directions where X-rays scattered by different atoms in the crystal are in phase, which in turn happens when the path difference (PD) between corresponding rays equals an integer number of wavelengths. Starting with rays scattered by different atoms in the same plane, these are, in analogy with the law of reflection, in phase (with PD $= 0$) when the incoming and outgoing angles, relative to the plane, are equal. Hence, by only studying reflection in crystallographic planes, we only need to consider the PD of rays reflected in different planes. According to the notations in Figure 11, the PD between two rays reflected in two adjacent parallel planes is given by $\mathrm{PD} = \mathrm{BC} + \mathrm{CD} = \mathrm{AC}\sin(\theta) = \mathrm{d}\sin(\theta)$. Hence, we get diffraction in directions where $\mathrm{d}\sin(\theta) = \mathrm{m}\lambda$. This is called *Bragg's law*.

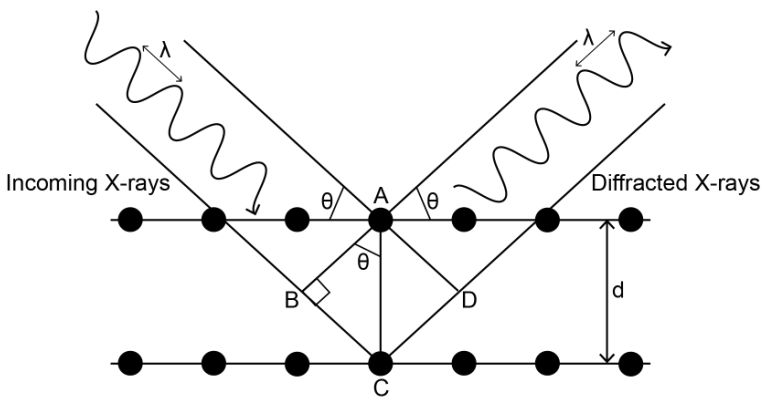

Figure 11: Schematic drawing of X-ray diffraction in a crystalline material. When the incoming X-rays scatter in phase with each other, diffraction occurs and Bragg's law is satisfied.

The Laue Description of Diffraction

There are two different ways to describe diffraction; Bragg's law, which is used for powders, and polycrystalline samples, and the *Laue formalism* which is typically used in SXRD. In the Laue formalism we describe the scattering in terms of the *reciprocal lattice* and *reciprocal space* (also known as *K space*).

As described by Equation 1 above, the atomic positions in a crystal can be described by the lattice points, which are connected by the lattice vectors $\mathbf{R} = n_1\mathbf{a} + n_2\mathbf{b} + n_3\mathbf{c}$. To every such lattice in real space, there is a corresponding so-called reciprocal lattice, which is the Fourier transform[15] of the real lattice and described by $\mathbf{G} = p_1\mathbf{a}^* + p_2\mathbf{b}^* + p_3\mathbf{c}^*$, where p_i are integers and the basis vectors are defined by Equation 9. In the same way that **a**, **b**, and **c** (Equation 1) span real space, $\mathbf{a}^*$, $\mathbf{b}^*$, and $\mathbf{c}^*$ (Equation 8) span reciprocal space. [73]

$$\mathbf{G} = p_1\mathbf{a}^* + p_2\mathbf{b}^* + p_3\mathbf{c}^*, \quad p_1, p_2, p_3 \in Z \tag{8}$$

$$\begin{cases} \mathbf{a}^* = 2\pi\frac{\mathbf{b}\times\mathbf{c}}{\mathbf{a}\cdot(\mathbf{b}\times\mathbf{c})} \\ \mathbf{b}^* = 2\pi\frac{\mathbf{c}\times\mathbf{a}}{\mathbf{a}\cdot(\mathbf{b}\times\mathbf{c})} \\ \mathbf{c}^* = 2\pi\frac{\mathbf{a}\times\mathbf{b}}{\mathbf{a}\cdot(\mathbf{b}\times\mathbf{c})} \end{cases} \tag{9}$$

To understand the relation between diffraction and the reciprocal lattice we use Figure 12, which shows two rays of an X-ray beam being scattered by two atoms. The incoming X-ray and the scattered X-ray are described by the *wave-vectors* $\mathbf{k}$ and $\mathbf{k'}$, respectively. They have the same length, $|\mathbf{k}| = |\mathbf{k'}| = k$. It is given by

$$k = \frac{2\pi}{\lambda} = \frac{2\pi E}{hc} = \frac{E}{\hbar c} \tag{10}$$

where λ is the wavelength of the X-ray. The change of the wave-vector $\mathbf{Q} = \mathbf{k'} - \mathbf{k}$ in Figure 12 is given by

$$\mathbf{Q} = h\mathbf{a}^* + k\mathbf{b}^* + l\mathbf{c}^* \tag{11}$$

[15]Named after the French mathematician Jean-Baptiste Joseph Fourier $(1768 - 1830)$.

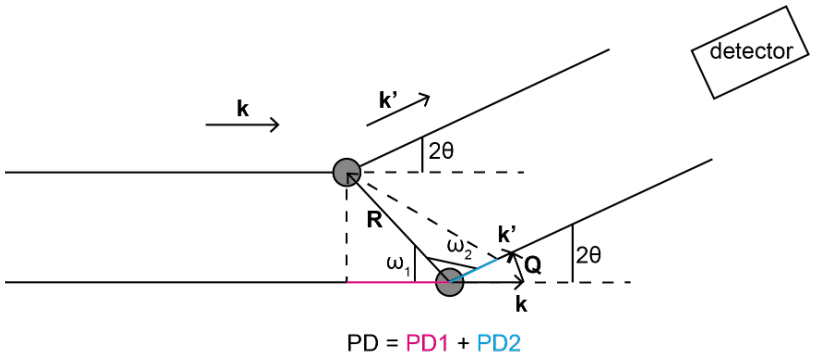

Figure 12: Schematic drawing of diffraction from two atoms.

Trigonometry gives us that

$$\begin{cases} \mathrm{PD1} = \mathrm{R}\cos(\omega_1) \\ \mathrm{PD2} = \mathrm{R}\cos(\omega_2) \end{cases} \tag{12}$$

The scalar products between $\mathbf{k}$ and $\mathbf{R}$ and between $\mathbf{k'}$ and $\mathbf{R}$ are given by

$$\begin{cases} \mathbf{k}\cdot\mathbf{R} = \mathrm{kR}\cos(180^\circ - \omega_1) = -\mathrm{kR}\cos(\omega_1) = -\mathrm{kPD1} \Rightarrow \mathrm{PD1} = -\frac{\mathbf{k}\cdot\mathbf{R}}{\mathrm{k}} \\ \mathbf{k'}\cdot\mathbf{R} = \mathrm{kR}\cos(\omega_2) = \mathrm{kPD2} \Rightarrow \mathrm{PD2} = \frac{\mathbf{k'}\cdot\mathbf{R}}{\mathrm{k}} \end{cases} \tag{13}$$

The PD between the two rays in Figure 12 becomes

$$\mathrm{PD} = \mathrm{PD1} + \mathrm{PD2} = -\frac{\mathbf{k}\cdot\mathbf{R}}{\mathrm{k}} + \frac{\mathbf{k'}\cdot\mathbf{R}}{\mathrm{k}} = \frac{\mathbf{R}}{\mathrm{k}}(\mathbf{k'} - \mathbf{k}) = \frac{\mathbf{R}\cdot\mathbf{Q}}{\mathrm{k}} \tag{14}$$

As mentioned previously, PD must equal an integer multiplied with the wavelength in order to have constructive interference. Since PD is also given by Equation 14, we get

$$\mathrm{PD} = \mathrm{m}\lambda = \frac{\mathbf{R}\cdot\mathbf{Q}}{\mathrm{k}} \Rightarrow \mathrm{m}\frac{2\pi}{\mathrm{k}} = \frac{\mathbf{R}\cdot\mathbf{Q}}{\mathrm{k}} \Rightarrow \mathbf{R}\cdot\mathbf{Q} = 2\pi\mathrm{m}, \quad \mathrm{m} \in \mathrm{Z} \tag{15}$$

Assuming that Equation 15 is valid, we can show that $\mathbf{Q} = \mathbf{G}$, which is called the *Laue condition*. Combining Equations 1, 11, and 15 gives

$$\mathbf{R}\cdot\mathbf{Q} = (\mathrm{n}_1\mathbf{a} + \mathrm{n}_2\mathbf{b} + \mathrm{n}_3\mathbf{c})(\mathrm{h}\mathbf{a}^* + \mathrm{k}\mathbf{b}^* + \mathrm{l}\mathbf{c}^*) = 2\pi\mathrm{m}, \quad \mathrm{m}, \mathrm{n}_1, \mathrm{n}_2, \mathrm{n}_3 \in \mathrm{Z} \tag{16}$$

This can be simplified to

$$n_1\mathbf{a}\cdot h\mathbf{a}^* + n_2\mathbf{b}\cdot k\mathbf{b}^* + n_3\mathbf{c}\cdot l\mathbf{c}^* = n_1 h(\mathbf{a}\cdot\mathbf{a}^*) + n_2 k(\mathbf{b}\cdot\mathbf{b}^*) + n_3 l(\mathbf{c}\cdot\mathbf{c}^*) \quad (17)$$

Since $\mathbf{a}\cdot\mathbf{a}^*$, $\mathbf{b}\cdot\mathbf{b}^*$, and $\mathbf{c}\cdot\mathbf{c}^*$ all equal 2π, we get

$$2\pi(n_1 h + n_2 k + n_3 l) = 2\pi m \Rightarrow n_1 h + n_2 k + n_3 l = m \quad (18)$$

In Equation 16, we see that m, n_1, n_2, and n_3 are integers, and thus, *(h,k,l)* must also be integers. In that case, Equation 11 must equal Equation 8: $\mathbf{Q} = \mathbf{G}$, *Q.E.D.*

We can also "go the other direction" and assume that $\mathbf{Q} = \mathbf{G}$ to show that $\mathbf{R}\cdot\mathbf{Q} = 2\pi m$. Since $\mathbf{Q} = \mathbf{G}$, we can write

$$\mathbf{R}\cdot\mathbf{Q} = \mathbf{R}\cdot\mathbf{G} = (n_1\mathbf{a}+n_2\mathbf{b}+n_3\mathbf{c})(p_1\mathbf{a}^*+p_2\mathbf{b}^*+p_3\mathbf{c}^*) = 2\pi(n_1p_1+n_2p_2+n_3p_3) \quad (19)$$

Since n_1, n_2, n_3, p_1, p_2, and p_3 are all integers, then $(n_1p_1+n_2p_2+n_3p_3)$ equals an integer, m, giving $\mathbf{R}\cdot\mathbf{Q} = 2\pi m$, *Q.E.D.*

Reciprocal space can be used for knowing what we see on the detector during SXRD. To determine which reflections that are visible on the detector at a certain sample-detector position, the *Ewald sphere construction*[16] is useful, see Figure 13.

In a 2D lattice, a circle with the radius k (the wave-vector, given by Equation 10) is drawn so that the origin, $(0,0)$, is on the perimeter and the incident beam vector, $\mathbf{k}$, starts in the center of the circle and ends at $(0,0)$, going in the incident beam direction. Then, the scattering vector, $\mathbf{k'}$, is drawn from the center of the circle to a lattice point, (x,y), on the perimeter. The reciprocal lattice vector, $\mathbf{Q}$, is drawn from $(0,0)$ to (x,y), and the scattering angle between $\mathbf{k}$ and $\mathbf{k'}$ is 2θ. By translating $\mathbf{k'}$ to start at $(0,0)$, one gets the direction in which the detector should be placed to detect (x,y), see Figure 13. As can be seen in Equation 10, the radius of the Ewald sphere is proportional to the X-ray energy, so the beam needs to be monochromatic. [73]

The cyan axes in Figure 13 indicate the $\mathbf{a}^*$ and $\mathbf{b}^*$ vectors in the reciprocal lattice. With their help, we can find out that the reflection observed on the detector is $(-1,2)$, since

$$\mathbf{Q} = -1\cdot\mathbf{a}^* + 2\cdot\mathbf{b}^* \quad (20)$$

[16]Named after the German physicist Paul Peter Ewald (1888 − 1985).

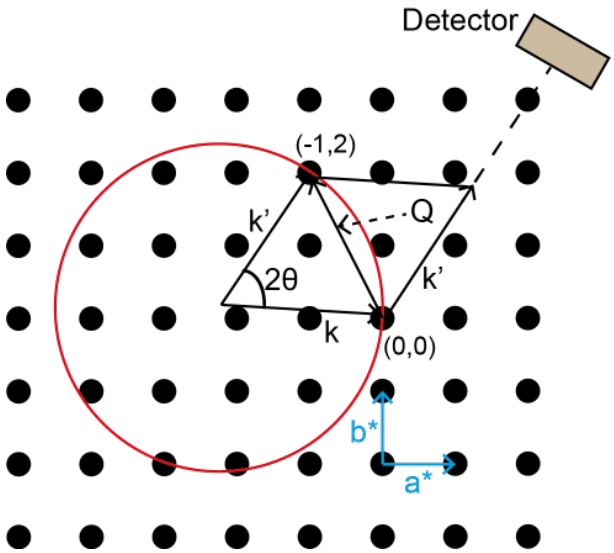

Figure 13: The Ewald sphere construction in 2D. The radius of the Ewald sphere is the length of the wave-vector, and it is proportional to the energy of the X-rays, see Equation 10. Here, the reflection at $(-1, 2)$ is detected. *Recreation of Figure 1 in [75].*

The law of cosines gives an expression for Q^2 (Equation 21) and thus Q (in Figure 13) is given by Equation 22. This can be rephrased to an expression for $\sin(\theta)$, see Equation 23. [73]

$$\mathrm{Q}^2 = \mathrm{k}^2 + \mathrm{k}^2 - 2\mathrm{k}\mathrm{k}\cos(2\theta) = 2\mathrm{k}^2(1 - \cos(2\theta)) = 2\mathrm{k}^2 2\sin^2(\theta) \tag{21}$$

$$\mathrm{Q} = 2\mathrm{k}\sin(\theta) = \frac{4\pi\sin(\theta)}{\lambda} \tag{22}$$

$$\sin(\theta) = \frac{\mathrm{Q}}{2\mathrm{k}} = \frac{1}{2\mathrm{k}}|\mathrm{h}\mathbf{a}^* + \mathrm{k}\mathbf{b}^* + \mathrm{l}\mathbf{c}^*| = \frac{1}{2\mathrm{k}}\sqrt{(\mathrm{h}a^*)^2 + (\mathrm{k}b^*)^2 + (\mathrm{l}c^*)^2} \tag{23}$$

For a cubic unit cell, Equation 23 can be written as

$$\sin(\theta) = \frac{\lambda}{2\mathrm{a}_0}\sqrt{\mathrm{h}^2 + \mathrm{k}^2 + \mathrm{l}^2} \Rightarrow \theta = \arcsin\left(\frac{\lambda}{2\mathrm{a}_0}\sqrt{\mathrm{h}^2 + \mathrm{k}^2 + \mathrm{l}^2}\right) \tag{24}$$

Structure Factor

The so-called *structure factor*, *F*, is given by

$$F^{\text{crystal}}(\mathbf{Q}) = \sum_j f_j(\mathbf{Q}) e^{i\mathbf{Q}\cdot\mathbf{r}_j} \sum_n e^{i\mathbf{Q}\cdot\mathbf{R}_n}, \quad i, j, n \in Z \tag{25}$$

where the first sum is called the *unit cell structure factor* and the second sum is called the *lattice sum*. The structure factor is proportional to the square root of the rod intensity ($F \propto \sqrt{I}$) and it is usually plotted as a function of *l*. [73]

Not all reflections are allowed in BCC and FCC structures (see Figure 2). We can use Equation 25 to find out which reflections will be allowed if we know the unit cell of the investigated material. For the BCC unit cell, the Miller indices for the atom in the center of the cell (the red atom in Figure 2b) are $(\frac{1}{2}, \frac{1}{2}, \frac{1}{2})$. For the FCC unit cell, the three lower red atoms in Figure 2c have the Miller indices $(0, \frac{1}{2}, \frac{1}{2})$, $(\frac{1}{2}, 0, \frac{1}{2})$, and $(\frac{1}{2}, \frac{1}{2}, 0)$. [73] When calculating the lattice sum, it is good to remember Euler's identity[17],

$$e^{i\pi\cdot x} = \begin{cases} 0 \text{ if } x \text{ is an odd integer} \\ 1 \text{ if } x \text{ is an even integer} \end{cases} \tag{26}$$

Inserting the Miller indices into Equation 25 shows the allowed reflections for BCC (Equation 27) and FCC (Equation 28), respectively. For BCC, the allowed reflections are the ones where the sum of *h,k,l* is even. For FCC, *h,k,l* must be either all even or all odd for the reflection to be allowed. [73]

$$\begin{aligned} \sum_n e^{i\mathbf{Q}\cdot\mathbf{R}_n} &= e^{i\mathbf{Q}\cdot 0} + e^{i\mathbf{Q}\cdot(\frac{1}{2}\mathbf{a}+\frac{1}{2}\mathbf{b}+\frac{1}{2}\mathbf{c})} = 1 + e^{i(h\mathbf{a}^*+k\mathbf{b}^*+l\mathbf{c}^*)\cdot(\frac{1}{2}\mathbf{a}+\frac{1}{2}\mathbf{b}+\frac{1}{2}\mathbf{c})} \\ &= 1 + e^{i(\frac{1}{2}h+\frac{1}{2}k+\frac{1}{2}l)2\pi} = 1 + e^{i\pi(h+k+l)} = \begin{cases} 2 \text{ if } h+k+l \text{ is even} \\ 0 \text{ if } h+k+l \text{ is odd} \end{cases} \end{aligned} \tag{27}$$

$$\begin{aligned} \sum_n e^{i\mathbf{Q}\cdot\mathbf{R}_n} &= e^{i\mathbf{Q}\cdot 0} + e^{i\mathbf{Q}\cdot(\frac{1}{2}\mathbf{a}+\frac{1}{2}\mathbf{b})} + e^{i\mathbf{Q}\cdot(\frac{1}{2}\mathbf{a}+\frac{1}{2}\mathbf{c})} + e^{i\mathbf{Q}\cdot(\frac{1}{2}\mathbf{b}+\frac{1}{2}\mathbf{c})} \\ &= 1 + e^{i(\frac{1}{2}h+\frac{1}{2}k)2\pi} + e^{i(\frac{1}{2}h+\frac{1}{2}l)2\pi} + e^{i(\frac{1}{2}k+\frac{1}{2}l)2\pi} \\ &= 1 + e^{i\pi(h+k)} + e^{i\pi(h+l)} + e^{i\pi(k+l)} = \begin{cases} 4 \text{ if } h,k,l \text{ are all even or all odd} \\ 0 \text{ if } h,k,l \text{ are mixed even and odd} \end{cases} \end{aligned} \tag{28}$$

[17] Named after the Swiss mathematician Leonhard Euler (1707 − 1783).

So, Equations 27-28 indicate that for a BCC lattice, the sum of *h,k,l* must be even for an allowed reflection, while for a FCC lattice, *h,k,l* must be either all even or all odd, and not mixed, to have an allowed reflection. BCC in real space is FCC in reciprocal space and vice versa (the crystal structure in real space is considered when calculating allowed reflections). [73]

How about SC, then? Well, since the SC unit cell has one atom with Miller indices $(0, 0, 0)$, we get a structure factor of 1 (Equation 29). Thus, all integer reflections are allowed for SC.

$$\sum_n e^{i\mathbf{Q}\cdot\mathbf{R}_n} = e^{i\mathbf{Q}\cdot 0} = 1 \tag{29}$$

Crystal Truncation Rods

In an infinite 3D crystal, scattering is isotropic, producing distinct reflections. The aim of SXRD, however, is to study surfaces, and in order to maximise the surface signal, the penetration depth is limited by letting the beam hit the surface at grazing incidence. Due to the broken periodicity at the surface, the scattering is non-isotropic. This entails so-called *crystal truncation rods* (CTRs) perpendicular to the surface. [73]

Why does the truncated surface of the crystal cause streaks instead of point-like intensities? To understand this, we recall Equation 15, but changing $\mathbf{R}$ from a 3D bulk vector to a 2D surface vector, such as in Equation 2. However, $\mathbf{Q}$ is still 3D due to scattering in all directions. This gives us that

$$\mathbf{R}\cdot\mathbf{Q} = (n_1\mathbf{a} + n_2\mathbf{b})\cdot(h\mathbf{a}^* + k\mathbf{b}^* + l\mathbf{c}^*) = 2\pi(n_1 h + n_2 k) \tag{30}$$

Now l does not have to be an integer anymore, so instead of point-like reflections, we get rods along the whole l range.

Figure 14 shows the ideal rods obtained from SXRD. A 3D infinite crystal would give intensity spikes at integer Q, almost like shifted Dirac delta functions[18] (cyan solid lines). If we cut a flat plane along the crystal to create a 2D half-infinite crystal, the intensity spikes "bleed towards" each other at low intensity, creating a wave-like function (green solid line). Besides CTRs – originating from the substrate bulk – there are also *surface rods* (SRs), giving information on which surface structures are available. A single layer – such as a superstructure on the substrate – would give rise to a relatively low, even intensity spanning all Q (magenta dashed line). [76]

[18]Named after the English theoretical physicist Paul Adrien Maurice Dirac (1902 – 1984).

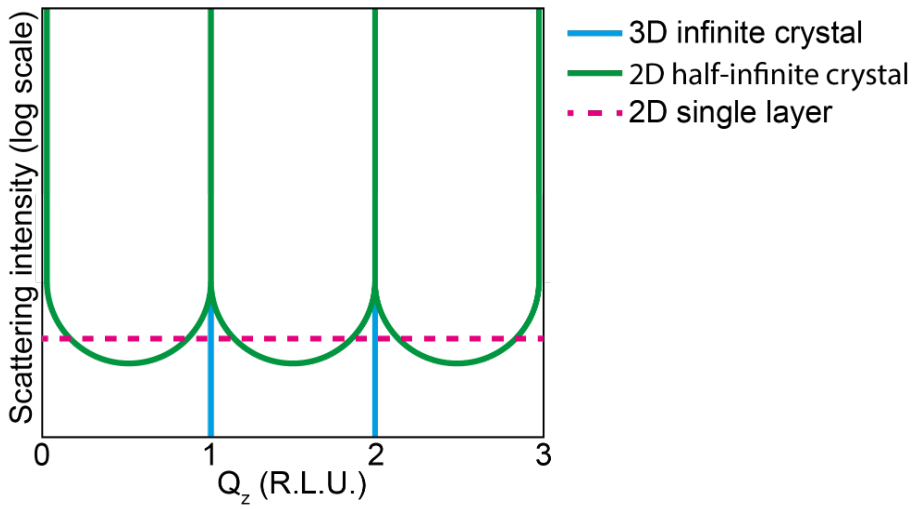

Figure 14: Schematic drawing of the ideal CTRs from a 3D infinite crystal (cyan) and a 2D half-infinite crystal (green) – i.e. basically a thick sample with a flat plane – and ideal SR from a 2D single layer (magenta). *Recreation of Figure 2 in [76].*

Since the bonds to surrounding atoms change at the surface, the top layers typically relax in the vertical direction. The shape of the CTRs are very sensitive to this. Generally, if the surface expands, the minima shift towards higher Q, and if the surface is compressed, the minima shift towards lower Q. [76]

An example of real CTRs is shown in Figure 15. The structure factors of the CTRs extracted from a clean $Pt_{25}Rh_{75}(100)$ single crystal (used in Paper I and Paper II) are plotted as functions of l. Even though the bulk is FCC, the surface is BC (compare to Figure 4a, where the first and second layers form the base of BC). According to Equation 27, $h+k+l$ must be even for the reflection to be allowed. Thus, $(h,k) = (1,0)$ (black) has a maximum at $l = 1$, while $(h,k) = (1,1)$ (red) has a minimum at the same l. Continuing towards higher l, the $(1,0)$ will have maxima at $l = 3, 5, 7$ etc. and the $(1,1)$ will have maxima at $l = 2, 4, 6$ etc. The discontinuity in the $(1,0)$ is caused by a tungsten piece.

Figure 16 illustrates schematically the principle for translating the crossing of CTRs with the Ewald sphere into detector images. Figure 16a shows a scatter plot with reflections allowed for the FCC lattice (see Equation 28) indicated as red discs connected with red lines. A small part of the Ewald sphere (assuming high X-ray energy) is depicted as a light blue rectangle with rounded edges. When the sample rotates, the Ewald sphere rotates with it, cutting the CTRs. A detector image is created, see Figure 16b, where the Bragg reflections are very bright (about 10^7 times brighter than the CTRs). Therefore, their positions on the detector need to be covered with tungsten pieces, in order to not destroy the detector pixels. Without the protection from the tungsten pieces, the detector could

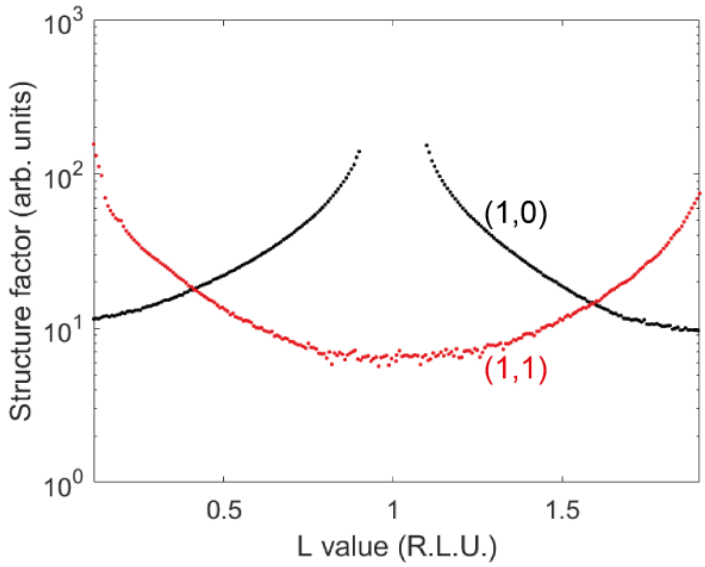

Figure 15: The $(1,0)$ (black) and $(1,1)$ (red) CTRs of a clean $Pt_{25}Rh_{75}(100)$ single crystal. At $l = 1$, there is a maximum for $(1,0)$ and a minimum for $(1,1)$. The discontinuity is caused by a tungsten piece protecting the detector from the high-energy Bragg reflection.

be burnt out due to over-saturated pixels (this is usually only a problem in HESXRD). The CTRs on the left side of Figure 16b correspond to the CTRs crossing the Ewald sphere in the left part of Figure 16a, and vice versa. [77] CTRs and SRs can also be displayed in an in-plane map, see Figure 16c. The *h,k* plane is here viewed along the *l* axis. The sample is a $Pt_{25}Rh_{75}(100)$ single crystal with a superstructure. Besides the Bragg reflections for the $(1,0)$ and $(1,1)$ (black circles), a (3×1) structure (white circles) can be seen. Note that since this is an image of reciprocal space, there are reflections at $(\frac{1}{3},1)$ and $(\frac{2}{3},1)$.

Analysing CTRs provides information about the atomic structure, even for very thin films (< 10 nm) [76]. The rod intensity is proportional to the square of the atomic number, i.e. $I \propto Z^2$. This means that heavy elements give rise to much more intense CTRs and SRs than light elements. However, we may still detect the presence of light elements on the surface. For instance, even though X-rays are not very sensitive to O atoms compared to heavier metal atoms [72], structure changes caused by oxygen induced segregation can be discovered by SXRD.

If there is line broadening in the rods, it is a sign of domains on the crystal. It is possible

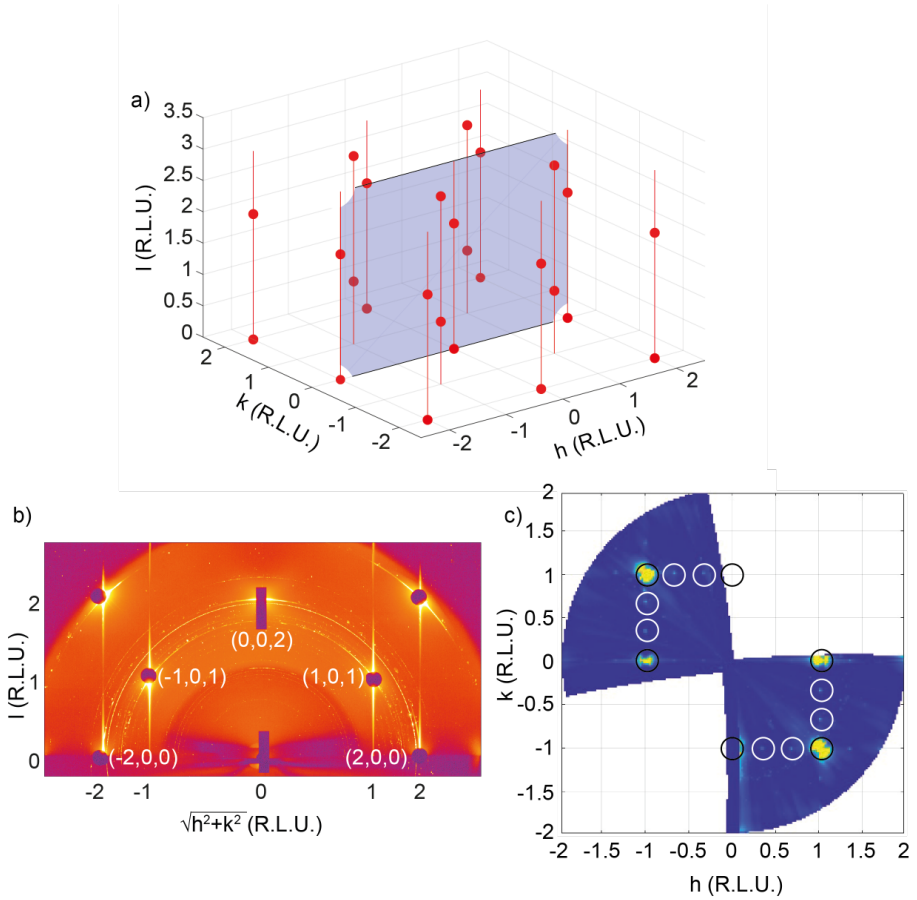

Figure 16: (a) Schematic plot of CTRs crossing the Ewald sphere during rotation. *Recreation of Figure 2d in [38].* (b) Maximum intensity HESXRD image with CTRs of a clean $Pt_{25}Rh_{75}(100)$ single crystal. *Recreation of Figure 2a in [38].* (c) In-plane map displaying the (3×1) structure on $Pt_{25}Rh_{75}(100)$. The black circles mark the Bragg reflections and the white circles mark the superstructure.

to calculate the average size of these domains by using the Scherrer equation[19],

$$\tau = \frac{K\lambda}{\beta \cos\theta} \tag{31}$$

where τ is the average domain size, K is a dimensionless shape factor ≈ 1, λ is the X-ray wavelength, β is the line broadening at the FWHM (full width at half maximum) of the rod after subtracting the instrumental broadening (unit: rad), and θ is the Bragg angle. [57]

[19]Named after the Swiss physicist Paul Scherrer (1890 – 1969).

SXRD Setup

Figure 17 shows the SXRD setup. X-rays hit the atoms in the sample and diffract towards a detector while the sample is rotating around its perpendicular axis. To maximise the surface-to-bulk signal, the sample is tilted at a low grazing incidence angle smaller than the critical angle of total reflection (for X-rays, the refraction index is lower than 1 and we can get external total reflection instead of internal total reflection as we get for visible light). The incidence angle is also shown in Figure 17, and it is usually very small, about $0.05 - 0.2°$ depending on the X-ray energy (higher energy entails lower critical angle).

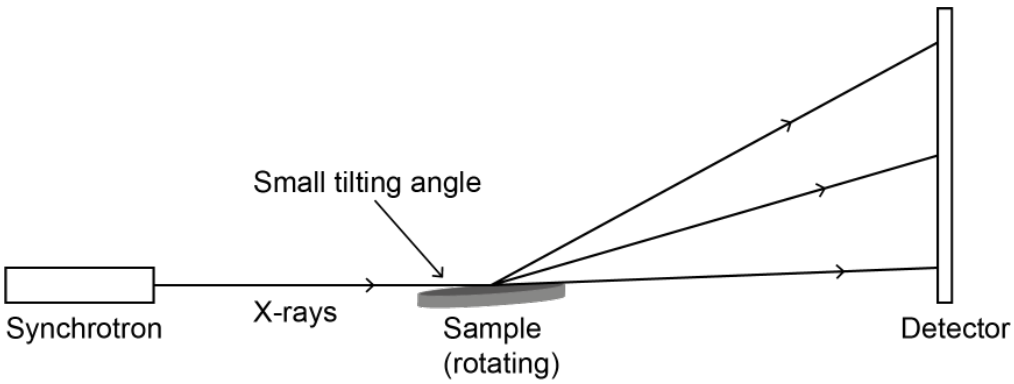

Figure 17: Schematic drawing of the SXRD setup.

Conventional SXRD uses an X-ray energy in the range of $10 - 20$ keV, while HESXRD uses X-rays with much higher energy ($>\sim 70$ keV). As can be seen in Equation 10, the wave-vector is proportional to the energy ($k \propto E$), and thus higher X-ray energy entails a larger and "flatter" Ewald sphere, displaying a larger part of the reciprocal space. [75, 77] For this thesis, most HESXRD experiments have been conducted at the Swedish Materials Science Beamline (P21.2) [12] at PETRA III, DESY in Hamburg, Germany.

When X-ray diffraction is made on polycrystalline thin film samples, as in Paper IV, it is called *grazing incidence X-ray diffraction* (GIXRD). The main difference between SXRD and GIXRD is that the latter is used for samples consisting of so many crystallites of different orientation that the CTRs generally cannot be observed, since they will go in all directions. One cannot study the surface structure in such samples, since CTRs are needed for that and the surface signal is too widely spread to be seen. Otherwise, SXRD and GIXRD have the same operating principles. [78]

Transmission Surface Diffraction

Transmission surface diffraction (TSD) is a technique that reminds of SXRD, but instead of hitting the sample at a low grazing incidence angle, the X-ray beam is penetrating the sample. The transmission mode has some advantages compared to conventional SXRD. By letting the X-rays travel straight through the sample, a larger part of the reciprocal space can be accessed in one measurement, with less bulk scattering and shorter acquisition time (though the time aspect is less of a problem in HESXRD). The in-plane atomic arrangement can be imaged directly and the interfaces can be investigated, e.g. the interface between Pd and PdO. The sample is mounted orthogonally to the beam, see Figure 18. [79, 80] The measurements were performed at the High-Energy Beamline for Buried Interface Structure and Materials Processing (ID31) [24] at ESRF in Grenoble, France, before I started my PhD.

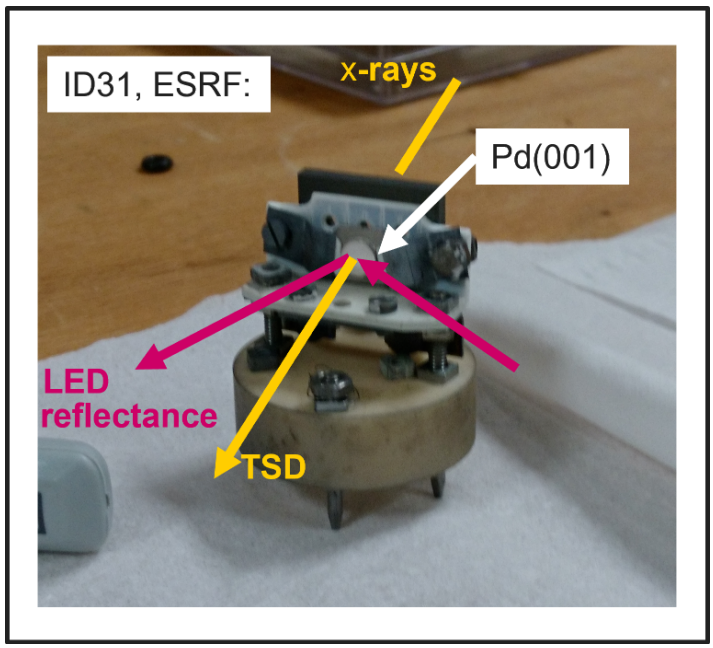

Figure 18: A TSD sample holder with a Pd(001) single crystal inserted.

Figure 4 in Paper III shows a TSD image displaying epitaxial PdO(100) on Pd(100). First, an image was recorded at reducing conditions. Then, the conditions were gradually changed to be very oxidising, and a new image was recorded. The "reduced" image was subtracted from the "oxidised" image, to remove background. The result of this image subtraction is a pattern where the diffraction spots for epitaxial PdO(100) on Pd(100) are indicated with red circles, which have larger radii for reflections with higher expected intensity.

Low Energy Electron Diffraction

Low energy electron diffraction (LEED) is a standard technique for determining the surface structure of crystalline samples. The first LEED experiment was performed in 1927 by the American physicists Clinton Davisson $(1881-1958)$ and Lester Germer $(1896-1971)$ [81], where they confirmed the *de Broglie hypothesis*[20],

$$\lambda = \frac{\mathrm{h}}{\sqrt{2\mathrm{m_e E}}} \Rightarrow \lambda(\text{Å}) \approx \sqrt{\frac{150.6}{\mathrm{E(eV)}}} \tag{32}$$

that tells us that particles are also waves. Here, λ is the wavelength of the electron, h is Planck's constant, m_e is the electron mass, and E is the kinetic energy of the electron beam. [33]

The LEED setup is shown in Figure 19. An electron gun emits a monochromatic electron beam with an energy somewhere in the range of $0-1$ keV. The beam hits the sample and the electrons are diffracted and elastically back scattered towards a phosphor screen. The energy range where these electrons can be analysed is $20-1000$ eV (corresponding to a wavelength of $2.744-0.388$ Å, according to the simplification of Equation 32), and they have an inelastic mean free path (IMFP) of $5-20$ Å. Before reaching the screen, the electrons travel through four concentric grids. Grids 1 and 4 are earthed in order to create a field free region. Grids 2 and 3 filter away inelastically scattered electrons, so that only elastically scattered electrons reach the screen. [33]

Figure 20 shows LEED measurements on a $Pt_{25}Rh_{75}(100)$ single crystal. When the crystal is clean (Figure 20a), a simple (1×1) structure is seen. After oxidising the crystal, a (3×1) superstructure forms (Figure 20b). LEED gives an image of the reciprocal lattice. Comparing Figure 20b to the HESXRD in-plane map in Figure 16c, one can see the similarity in the diffraction pattern.

[20] Named after the French physicist and aristocrat Louis-Victor Pierre Raymond de Broglie $(1892-1987)$.

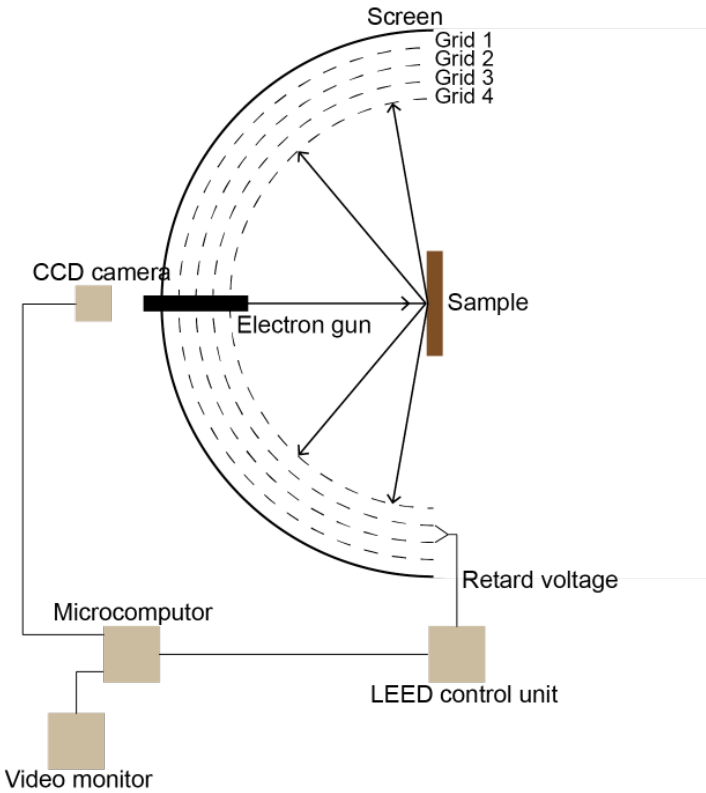

Figure 19: Schematic drawing of the LEED setup. *Recreation of Figure* 2.13 *in [33].*

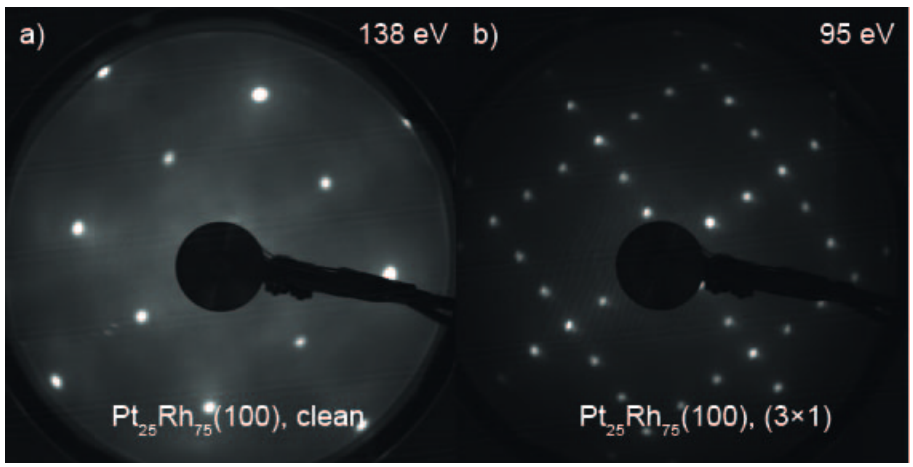

Figure 20: LEED images captured on a $Pt_{25}Rh_{75}(100)$ single crystal in clean state (a), and with a (3×1) superstructure with O (b).

Ambient-Pressure X-Ray Photoelectron Spectroscopy

X-ray photoelectron spectroscopy (XPS) is a technique that allows chemical analysis of surfaces. It is built upon the photoelectric effect, i.e. photon induced electron emission, see Figure 21. This effect was discovered by the German physicist Heinrich Hertz (1857 – 1894) in 1887 and explained by the German theoretical physicist Albert Einstein (1879 – 1955) in 1905, rendering him the Nobel Prize in Physics in 1921. In 1954, the Swedish physicist Kai Siegbahn (1918 – 2007) and coworkers used a high-resolution electron spectrometer to obtain spectra where the characteristic peaks of X-ray photoelectrons were clearly visible. This was the break-through of XPS, and Siegbahn received the Nobel Prize in Physics in 1981 for developing the electron spectroscopy for chemical analysis (ESCA). [82]

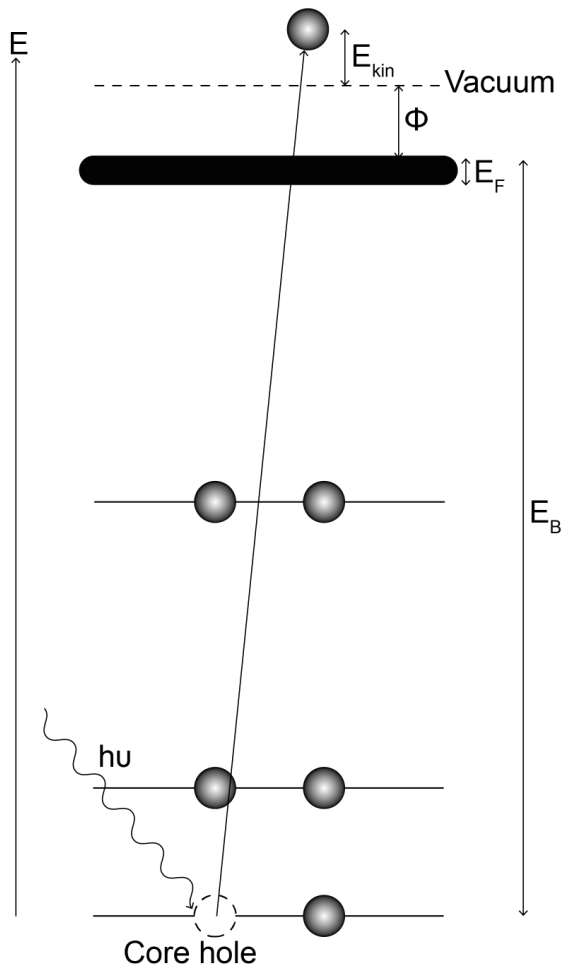

Figure 21: Schematic drawing of the principle of XPS. *Recreation of Figure* 2.3 *in [33].*

The principle of XPS is shown in Figure 21. An electron with the binding energy E_B in solid state is excited by the photon energy, $h\nu$. If this energy is high enough to move the electron higher than the *vacuum level*, the electron is emitted from the atom and gets the kinetic energy E_{kin}. The *Fermi level*[21], E_F, is the highest occupied state the electron can have without leaving the atom, and the energy difference between the vacuum level and the Fermi level is called the *work function*, Φ. [33] The E_B of the emitted electron is given by

$$E_B = h\nu - E_{kin} - \Phi \tag{33}$$

E_B is usually calibrated to E_F, and it is specific for different elements. E_B is also affected by the surroundings, e.g. for oxygen, we get slightly different E_B depending on if the oxygen exists as O_2 in the gas-phase, as part of an oxide, or as chemisorbed on the surface. This is called *chemical shifts* and depends on changes in the binding strength inside the atom as it reacts with other atoms in its surroundings. Similarly, atoms of the same element have different E_B depending on if they are in the bulk or in the surface. [33]

The XPS spectrum shows intensity as a function of E_B, but instead of sharp, well-defined lines, there are more or less broad peaks in the spectra. There are three broadening contributions to an XPS peak: *instrumental broadening*, *the excitation life time*, and *asymmetry*. The peak shape will be a convolution of these contributions.

The instrumental broadening is due to imperfections in the experimental setup, as well as the "human factor". It gives rise to a Gaussian shape[22] of the peak. The excitation life time is the time between excitation and deexcitation of an electron. According to *Heisenberg's uncertainty principle*[23],

$$\Delta E \cdot \Delta t \geq \hbar \tag{34}$$

we cannot measure both energy and time with great precision. Due to a limited life time (Δt), the measured binding energy (ΔE) is not infinitely sharp, rather the peak gets a Lorentzian shape[24]. The asymmetry of the XPS peak is caused by small excitations around the Fermi level, and together with the Lorentzian, it causes the so-called *Doniach-Šunjić (D-S) line shape*[25] [83].

[21]Named after the Italian physicist Enrico Fermi (1901 − 1954).

[22]Named after the German mathematician, geodesist, and physicist Carl Friedrich Gauss (1777 − 1855).

[23]Named after the German physicist Werner Heisenberg (1901 − 1976).

[24]Named after the Dutch physicist Hendrik Lorentz (1853 − 1928).

[25]Named after the British-American physicist and professor Sebastian Doniach (b. 1934) and the Croatian physicist, professor, and diplomat Marijan Šunjić (b. 1940).

The XPS software needs the following input: binding energy, intensity, instrumental broadening, life time, asymmetry and background. Then it calculates a theoretical XPS spectrum that the experimental data can be compared to.

When elements transform into compounds, their XPS peaks may shift. For instance, the $Pd3d_{5/2}$ peak shifts a little upward when the Pd is oxidised [84]. Some peaks may overlap, e.g. the O1s and $Pd3p_{3/2}$ peaks [64], but that does not cause any problems to detect the surface oxide.

XPS is often performed in vacuum, but it is also possible to perform ambient-pressure XPS (APXPS). The presence of the many molecules in the surrounding gas-phase hinders the photons are from reaching the detector. To overcome this problem, the distance between the sample and the analyser is kept as short as possible. Inside the analyser, there are several vacuum chambers with pumps, lowering the pressure more and more until the pressure at the detector is about 10^{-8} mbar. The orifices between the chambers and at the muzzle of the analyser are very small, so electronic lenses are needed to focus the beam and avoid scattering.

We have performed APXPS measurements on $PdAu/Al_2O_3(0001)$ at the Ambient-Pressure Soft X-ray Photoelectron Spectroscopy (Beamline 9.3.2) [27, 28, 29] at ALS (Advanced Light Source) in Berkeley, San Francisco in California, USA.

Density Functional Theory

The electronic structure of atoms, molecules, and solids can be calculated using *density functional theory* (DFT). This computational method is built on the fundamental laws of quantum mechanics and can provide a quantitative understanding of materials properties. [85] The DFT calculations in this thesis have not been done by me – they were performed by Dr. Henrik Grönbeck at Chalmers University in Gothenburg, Sweden – but as DFT has been used in Paper I and Paper II in order to calculate the atomic positions in different surface configurations on $Pt_{25}Rh_{75}(100)$, a short introduction to the basics of DFT is included in this thesis.

As the name suggests, DFT uses the electron density in a system to calculate its total energy. Consider a system with M nuclei and N electrons. The energy of the system is described by the electronic wave-function, $\Phi(\mathbf{R}_1, ..., \mathbf{R}_M, \mathbf{r}_1..., \mathbf{r}_N)$. The nuclei and electrons in the system have kinetic energy (T_{nucl} and T_{el}, respectively) and the electrostatic field of the nuclei has potential energy from interacting with each other and with the electrons ($V_{nucl-nucl}$ and $V_{nucl-el}$, respectively). There is also potential energy from the interactions between the

electrons (V_{el-el}). The sum of these contributions defines the *Hamiltonian operator*[26] ($\mathcal{H}$) of the system, see Equation 35. [86]

$$\mathcal{H} = T_{nucl} + T_{el} + V_{nucl-nucl} + V_{nucl-el} + V_{el-el} \tag{35}$$

Having the Hamiltonian, the total energy is obtained by solving the *Schrödinger equation*[27]. We can solve the Schrödinger equation (Equation 36) if the wave-function Φ is known. [86]

$$\mathcal{H}\Phi(\mathbf{R}, \mathbf{r}) = E\Phi(\mathbf{R}, \mathbf{r}) \tag{36}$$

However, because of the *Pauli principle*[28], which states that each electron must have a unique state, and the many-body character of the V_{el-el} interaction, the Schrödinger equation can be solved analytically only for one-electron systems. Thus, methods have been developed to solve the Schrödinger equation numerically. [86]

A first step to solve the Schrödinger equation is to apply the *Born-Oppenheimer approximation*[29] in which nuclei and electrons are treated separately. This is a reasonable approximation as the electron is much lighter and much faster than an atom (with $Z \geq 3$). Thus, the first step is to assume fixed positions for the atoms and to solve the Schrödinger equation for the electrons in the external potential of the nuclei. [86]

The three persons who laid the foundation to DFT were the French-American theoretical physicist Pierre C. Hohenberg ($1934-2017$), the Austrian-American theoretical physicist and theoretical chemist Walter Kohn ($1923-2016$), and the American physicist Lu Jeu Sham (b. 1938) [85]. They worked out the theoretical framework during the 1960's, which has made DFT a feasible method for solving surface related problems. Hohenberg and Kohn showed that in an inhomogeneous electron gas, where the electrons interact with each other in an external potential, the potential is determined by the ground state electron density so that the energy in the system is minimised [87]. One year later, Kohn and Sham developed the theory and suggested that instead of trying to calculate the electron density in a many-electron system, the electron density can be obtained by calculating a set of self-consistent single-electron equations [88].

There are several different software, which have implemented DFT for electronic structure

[26]Named after the Irish mathematician, astronomer, and physicist William Rowan Hamilton ($1805-1865$).

[27]Named after the Austrian-Irish physicist Erwin Schrödinger ($1887-1961$).

[28]Named after the Austrian theoretical physicist Wolfgang Ernst Pauli ($1900-1958$).

[29]Named after the German-British physicist and mathematician Max Born ($1882-1970$) and the American theoretical physicist Julius Robert Oppenheimer ($1904-1967$).

calculations of molecules, surfaces, and bulk materials. The software used for the calculations in this thesis is VASP (Vienna *Ab-initio* Simulation Package) [89, 90, 91].

Summary of Papers

Paper I: The (3×1) and c(8×2) Oxygen Structures Formed on a $Pt_{25}Rh_{75}$(100) Model Catalyst During CO Oxidation

We performed CO oxidation as a model reaction on a $Pt_{25}Rh_{75}(100)$ model catalyst during a commissioning beamtime. We found three different structures, namely a (3×1) reconstruction with chemisorbed O under mildly oxidising conditions, a $c(8 \times 2)$ surface oxide under strongly oxidising conditions, and a $c(2 \times 2)$ surface structure under reducing conditions and elevated temperature. This paper describes the oxygen structures, while the $c(2 \times 2)$ structure is described in Paper II.

The (3×1) and $c(8 \times 2)$ surfaces are previously known to form on both Rh(100) [51, 58, 66, 67, 92] and PtRh(100) [15, 16, 19, 63, 65]. Quantitative analysis of SXRD has been done for the $c(8 \times 2)$ on both pure Rh(100) [66] and on $Pt_{25}Rh_{75}(100)$ [58]. Quantitative LEED analysis has been done on (3×1) on $Pt_{25}Rh_{75}(100)$ [16], but to our knowledge, the (3×1) rods obtained by SXRD have not been analysed quantitatively on PtRh(100).

DFT calculations were used to optimise the atomic positions in the (3×1) reconstruction with chemisorbed O and a $c(8 \times 2)$ surface oxide on PtRh(100). Then CTRs and SRs of these structures were simulated and compared to the experimental data. We got well-fitting rods for (3×1), the simulations shown in Figure 2 in Paper I are not optimised further. The (3×1) is a "shifted row" reconstruction, where Rh has segregated to the surface, every third atomic row in the top Rh layer is shifted by half the surface lattice constant and oxygen atoms are adsorbed in the resulting three-fold hollow sites to a coverage of 2/3 ML, in perfect agreement with previous studies [16, 66].

However, the $c(8 \times 2)$ proved more difficult to fit. Figure 4 in Paper I shows that we did not get a good fit for the expected trilayer surface oxide. However, we got reasonable agreement when we simulated three different structures coexisting at the surface. These structures were: (i) a metallic surface, (ii) the trilayer surface oxide, and (iii) two trilayers stacked on top of each other, separated by a sparse Rh layer. When optimised, these three

structures occupied the surface to the following extent: (i) 32%, (ii) 46%, and (iii) 22%, with a 34% occupancy of the sparse layer, which well within error margins match 1/3 as Gustafson et al. [93] suggested for a corresponding structure. Thus, the best fit for the c(8 × 2) structures is a combination of the normal trilayer surface oxide, a double trilayer separated by a sparse Rh layer, and a metallic surface.

The results in Paper I shows that the well-documented oxygen structures on PtRh(100) can be analysed quantitatively.

Paper II: A c(2×2) Reconstruction of $Pt_{25}Rh_{75}(100)$

This manuscript is the "second part" of Paper I, providing a status report for the determination of the unexpected c(2×2) structure on $Pt_{25}Rh_{75}(100)$ under reducing conditions and elevated temperature. We have not yet found any satisfying fit for the CTRs and SRs in the experimental data, which also agrees with DFT calculations. However, for this thesis, we describe what we have done so far and what hypotheses we have tried, as well as comment on the best fit we have obtained so far.

Initially, our interpretation was that CO adsorbed in atop sites in a c(2 × 2), with a preference for Rh atoms, hence inducing ordering of the surface layer. Analysis of the SRs, however, made it clear that the structure is not a simple surface structure, but it extends about 3 layers into the sample.

Several different surface configurations were simulated, and the best fit, shown in the manuscript, looks very good. The corresponding model consists of a top layer with slightly enrichment in Pt. The c(2 × 2) ordering is mainly seen in the third layer, which correspondingly has a Pt:Rh ratio very close to 50:50. The second layer is very Pt rich, while layers 1, 4, and 5 show smaller enrichment in Pt. All these five layers show a tendency to display c(2 × 2), while below these, the layers have a random bulk mixture. It is probably not realistic to have this much Pt in the near-surface region, as the alloy has a Pt:Rh ratio of 1:3. Hence, the work is still ongoing.

Although the c(2×2) structure is not solved yet, this study emphasises one of the strengths with HESXRD, or rather the use of a large 2D detector. If we had used a conventional SXRD setup, we would probably not have discovered the c(2 × 2) SRs, since a much smaller part of the reciprocal space would have been imaged on the detector.

Paper III: Formation of Epitaxial PdO(100) During the Oxidation of Pd(100)

In this paper, the oxidation of Pd(100) was studied by TPD, LEED, and *in situ* TSD. It was found that an epitaxial, multilayer PdO(101) structure forms at 500 K[30], but if the oxidation starts at a temperature above 600 K, an epitaxial PdO(100) structure grows together with the PdO(101) structure. The lattice vectors of PdO(101) are rotated 26.6° relative to the lattice vectors of the substrate to minimise the strain needed to fit the substrate. Thus, the thin PdO(101) has a $(\sqrt{5} \times \sqrt{5})$R27° unit cell with respect to the Pd(100) lattice. This rotation is not observed for PdO(100) on Pd(100). The oxide forming at higher temperature becomes thicker (15 ML compared to 5.5 ML), more rough, more heterogeneous, and less stable, since it decomposes at lower temperature. The explanation to the different oxidation behaviours at different temperatures is that the stability of small PdO domains changes with temperature. Only PdO domains that are large enough grow into a thick PdO(100) film under meta-stable nucleation conditions.

Paper IV: Alloying and Oxidation of PdAu Thin Films

The idea of this study is based on a methane oxidation study on a Pd(100) single crystal from 2012 by Hellman et al. [4]. The catalytic activity was found to increase with increasing temperature and oxide thickness up to a certain point, and then the activity decreased while the oxide continued to grow thicker, even though the temperature was still increasing. When the oxide decomposed, however, the catalytic activity increased again. A possible explanation is that the thin PdO film exposes the catalytically active (101) orientation, but when the oxide grows thick enough, it exposes the (100) orientation, which is catalytically low-active (compare to Paper III).

By alloying Pd with an inert metal such as Au, is it then possible to limit the oxide growth compared to pure Pd and stabilise PdO(101) instead of PdO(100)? This was the scope of our paper. We studied bimetallic thin film samples, consisting of a sapphire substrate with a Pd film and an Au film deposited on top, using GIXRD at P21.2 [12] to find out when alloying and oxidation occurred.

As expected, PdAu is more difficult to oxidise compared to pure Pd. However, the impairing effect on PdO formation by Au was surprisingly large. Pure Pd was oxidised at an O_2 pressure of 1.5 mbar, while the O_2 had to be increased to 10 mbar to oxidise $Pd_{15}Au_{05}$ and $Pd_{10}Au_{10}$. $Pd_{05}Au_{15}$ could not be oxidised even at 500 mbar O_2. When Pd was deposited

[30]Named after the British mathematician, mathematical physicist, and engineer William Thomson, a.k.a. Lord Kelvin, (1824 − 1907).

on top of Au, the sample became more easily oxidised.

The degree of ordering was estimated for both the metallic phase and the oxide phase, as well as the degree of oxidation. PdAu was found to be more ordered than pure Pd, and the preferential order was Pd(111). For the oxide to become well-ordered, annealing the sample in vacuum, prior to oxidation, was a requirement; in the cases where the sample had not been annealed prior to oxidation, the oxide did not show a preferential order. The dominating oxide orientation on most sample was (100), i.e. the surface orientation we hoped to avoid. However, it was found that higher Au concentration entails less oxide and more (100), while lower Au concentration entails a thin (101) oxide. Our best results were from the $Pd_{15}Au_{05}$ sample, where 95% of the metal and 64% of the oxide were ordered. The ordered oxide displayed 51% (101), 35% (100), and 14% (110).

One speculation from our side is that the changed lattice constant of the PdAu alloy compared to pure Pd causes stabilisation of another surface orientation, and if Pd was alloyed with another metal with a lattice constant more similar to that of Pd, perhaps PdO(101) would be stabilised. Pt and Pd have rather similar lattice constants, while that of Au is larger. Furthermore, according to theoretical calculations, Pt has positive segregation energy in a PdPt alloy while Au has negative segregation energy in a PdAu alloy, and thus Pt would segregate deeper into the bulk instead of towards the surface, as Au would [94]. Then the surface would be Pd enriched and easier to oxidise.

Paper v: Oxidation of PdAu Thin Films and the Subsequent Reduction by CH_4 and Heat

This APXPS study is a continuation of Paper iv. We oxidised a $Pd_{15}Au_{05}/Al_2O_3$ thin film sample and reduced the oxide with methane. We both oxidised the sample fully and formed a thin oxide.

In Paper iv, an O_2 pressure of 10 mbar was required to oxidise $Pd_{15}Au_{05}$, but in this study, oxidation happened at 1 mbar O_2. The reason for this was probably that the pressure was set before rapidly increasing the temperature. It was possible to reduce the oxide with methane. The reduction was slowed down as we reached an oxygen coverage corresponding to surface oxide, but as metallic patches were appearing, the rest of the oxide was reduced relatively quickly.

The thin oxide was destabilised by the presence of Au in the substrate and was reduced in vacuum at 280°C[31]. The oxide decomposed down to two layers.

[31]Named after the Swedish astronomer, physicist, and mathematician Anders Celsius (1701 − 1744).

Conclusions and Outlook

This thesis presents the results of oxidation catalysis on alloy model catalysts such as a $Pt_{25}Rh_{75}(100)$ single crystal (Paper I and Paper II) and $PdAu/Al_2O_3(0001)$ thin films (Paper IV and Paper V), as well as $PdO(100)$ formation on $Pd(100)$ (Paper III). Paper I shows the simulations of two well-known oxygen structures on the PtRh bimetallic system, namely a (3×1) reconstruction with chemisorbed O (formed under mildly oxidising conditions) and a $c(8 \times 2)$ surface oxide (formed under strongly oxidising conditions). A third – unexpected – structure formed on the $Pt_{25}Rh_{75}(100)$ single crystal under reducing conditions and elevated temperature, namely a $c(2 \times 2)$ structure, which we attempted to analyse in Paper II (it proved to be more difficult than we expected). Paper III presents a LEED, TPD, and TSD study on CO oxidation over $Pd(100)$. Paper IV builds on the study by Hellman et al. [4] were they performed methane oxidation on $Pd(100)$ and realised that a thick PdO film lead to low catalytic activity. The aim of Paper IV was to limit the PdO thickness by using PdAu instead of pure Pd, but it turned out that among the various surface orientations we could observe, $PdO(100)$ was one of them. Paper V is a complement to Paper IV, an APXPS study of the PdAu thin film sample with the lowest Au concentration (25%).

The tools we have used to analyse the rods in Paper I and Paper II have their limitations. The softwares ANAROD [95] and WinROD [96] were used for the quantitative analysis of the rods. ANAROD can only handle two coinciding surface structures plus the bulk terminated surface, while WinROD can handle up to three surface structures simultaneously. Using another software that can handle more surface structures existing simultaneously could be an alternative. In Paper II, we describe our attempts to recreate the $c(2\times2)$ structure, which were less successful. However, if we would try with the same conditions and vary them a little, we could have the possibility to increase the understanding of when the $c(2 \times 2)$ structure forms on $PtRh(100)$.

PdAu was – not surprisingly – more difficult to oxidise than pure Pd. We had to "go back" from trying to oxidise CO or methane to expose the sample to only O_2, in order to form PdO. The PdO grown on the PdAu alloy was to a larger degree oriented as $PdO(100)$ than we expected. This might be related to the lattice constant which increases with the amount

of Au in the alloy (PdAu follows Vegard's law very well [97]). The ordering of the metallic phase was mostly (111), which is not as open as the (100) surface [34]. This may affect adsorption and catalytic behaviour, as it has been shown that PdAu(100) exhibits better catalytic activity for O_2 dissociation than PdAu(111), due to the more obstructing surface configuration of the latter, making it more difficult for the O_2 to adsorb and dissociate [98]. We have an idea of adjusting the alloy's lattice constant by using PdPt instead of PdAu, since Pt has a lattice constant closer to that of Pd. Then the lattice constant of the PdPt should not be too far from the Pd lattice constant. We have tried the same HESXRD experiments on PdPt/Al_2O_3(0001) as we did on PdAu/Al_2O_3(0001), though the results are not yet analysed to the degree that we can say if we could avoid PdO(100) or not. Another idea for future studies of the PdAu alloy is using lower Au concentration ($< 25\%$), since a low Au content in the PdAu alloy seems to entail a thinner PdO film and bigger probability of exposing the (101) surface orientation.

One thing I have thought about during beamtimes is a way to improve the alignment process. Aligning the crystal in the HESXRD chamber can be quite difficult. Especially when we are heating or cooling the sample, because of expansion and contraction. Then we may need to realign the sample before each measurement, as the temperature changes. I think it would be practical to have some kind of automatic alignment, such as a script you can run to let the computer do the alignment instead of the scientist doing it manually. Developing such a script might be troublesome, though. My programming skills are, at the time of writing, too rudimentary for me to tell whether the programming part would be difficult for a more experienced programmer, but testing the code could cause severe damage to the detector if some error causes the direct beam to burn the detector. It could be costly to develop an alignment script if it means we have to sacrifice detectors for this purpose. However, if we had an automatic alignment procedure, and it was trustworthy and secure, we could avoid bad measurements caused by bad alignment and get better and more reliable data out of our HESXRD measurements.

How far is the step from model catalysts to industrial catalysts? As described in the section *Model Catalysts* in the chapter *Surface Science and Catalysis*, the catalysts we study in the laboratory are not quite the same as the catalysts used in industry. The differences in materials, pressures, and complexity are quite large. Already in 1977, Sinfelt wrote the following [8]:

> "For a bimetallic catalyst to be of interest for industrial applications, it is necessary that it be prepared in a high surface area form and that it be resistant to loss of surface area during use."

If 1‰ of the atoms in the catalyst is a surface atom, then the surface area of that catalyst would be ~ 1 m^2/g [8]. To have this, we would need to have a finely ground powder. If we

take Pd as an example, with its lattice constant of 3.89 Å, and assume spherical particles, these particles would need a diameter of $\sim$ 2.3 µm. Thus, our single crystals and thin film samples have way too low surface-to-bulk ratio. This is why nanoparticles on the mesoscopic scale are used for industrial catalysts [31].

Trying to transition from ”lab conditions” to ”real conditions” and studying the catalytic-reactions-induced surface changes would be very demanding [15]. There are several orders of magnitude more particles at ambient pressure compared to UHV, and the sample would be significantly more dirty than under vacuum conditions. As is known, the surface composition differs significantly from the bulk composition [9] and bonds between the metal atoms and surrounding atoms, e.g. O, can cause unintended segregation of atoms where they are ”not supposed” to be [2].

Even if the materials and pressure gaps between model catalysts and industrial catalysts are still wide, every step to bridging them counts. Hopefully, we have managed to contribute to the understanding of surface reconstructions and how they can be utilised in catalysis research.

References

Bibliography

[1] S. Blomberg, J. Zetterberg, J. Gustafson, J. Zhou, C. Brackmann, and E. Lundgren. Comparison of AP-XPS and PLIF Measurements during CO Oxidation over Pd Single Crystals. *Topics in Catalysis*, 59(5-7):478–486, January 2016.

[2] John R. Kitchin, Spencer D. Miller, and David S. Sholl. Density functional theory studies of alloys in heterogeneous catalysis. In *Chemical Modelling*, volume 5, pages 150–181. RSC Publishing, November 2008.

[3] Johan Gustafson, Olivier Balmes, Chu Zhang, Mikhail Shipilin, Andreas Schaefer, Benjamin Hagman, Lindsay R. Merte, Natalia M. Martin, Per-Anders Carlsson, Maciej Jankowski, Ethan J. Crumlin, and Edvin Lundgren. The Role of Oxides in Catalytic CO Oxidation over Rhodium and Palladium. *ACS Catalysis*, 8(5):4438–4445, May 2018.

[4] A. Hellman, A. Resta, N. M. Martin, J. Gustafson, A. Trinchero, P. A. Carlsson, O. Balmes, R. Felici, R. van Rijn, J. W. M. Frenken, J. N. Andersen, E. Lundgren, and H. Grönbeck. The active phase of palladium during methane oxidation. *Journal of Physical Chemistry Letters*, 3(6):678–682, February 2012.

[5] Matthew T. Darby, Michail Stamatakis, Angelo Michaelides, and E. Charles H. Sykes. Lonely Atoms with Special Gifts: Breaking Linear Scaling Relationships in Heterogeneous Catalysis with Single-Atom Alloys. *Journal of Physical Chemistry Letters*, 9(18):5636–5646, September 2018.

[6] Nicholas Marcella, Jin Soo Lim, Anna M. Płonka, George Yan, Cameron J. Owen, Jessi E. S. van der Hoeven, Alexandre C. Foucher, Hio Tong Ngan, Steven B. Torrisi, Nebojsa S. Marinkovic, Eric A. Stach, Jason F. Weaver, Joanna Aizenberg, Philippe Sautet, Boris Kozinsky, Anatoly I. Frenkel, and Harvard A. John Paulson. Decoding

reactive structures in dilute alloy catalysts. *Nature Communications*, 13(832):1–9, February 2022.

[7] Se H. Oh and Joyce E. Carpenter. Platinum-rhodium synergism in three-way automotive catalysts. *Journal of Catalysis*, 98(1):178–190, March 1986.

[8] John H. Sinfelt. Catalysis by Alloys and Bimetallic Clusters. *Accounts of Chemical Research*, 10(1):15–20, January 1977.

[9] A. Jabloński, S.H. Overbury, and G.A. Somorjai. The Surface Composition of the Gold-Palladium Binary Alloy System. *Surface Science*, 65(2):578–592, July 1977.

[10] Feng Gao, Yilin Wang, and D. Wayne Goodman. CO Oxidation over AuPd(100) from ultrahigh vacuum to near-atmospheric pressures: CO adsorption-induced surface segregation and reaction kinetics. *Journal of Physical Chemistry C*, 113(33):14993–15000, July 2009.

[11] Feng Gao and D. Wayne Goodman. Pd–Au bimetallic catalysts: Understanding alloy effects from planar models and (supported) nanoparticles. *Chemical Society Reviews*, 41(24):8009–8020, November 2012.

[12] W. Drube, M. Bieler, W. A. Caliebe, H. Schulte-Schrepping, J. Spengler, M. Tischer, and R. Wanzenberg. The PETRA III extension. *AIP Conference Proceedings*, 1741(1), July 2016.

[13] Hans Joachim Freund, Gerard Meijer, Matthias Scheffler, Robert Schlögl, and Martin Wolf. CO oxidation as a prototypical reaction for heterogeneous processes. *Angewandte Chemie - International Edition*, 50(43):10064–10094, October 2011.

[14] A. Ramstad, F. Strisland, T. Ramsvik, and A. Borg. CO adsorption on the Pt/Rh(100) surface studied by high-resolution photoemission. *Surface Science*, 458(1):135–146, June 2000.

[15] U. Hejral, D. Franz, S. Volkov, S. Francoual, J. Strempfer, and A. Stierle. Identification of a Catalytically Highly Active Surface Phase for CO Oxidation over PtRh Nanoparticles under Operando Reaction Conditions. *Physical Review Letters*, 120(12):126101, March 2018.

[16] M. Sporn, E. Platzgummer, E. L.D. Gruber, M. Schmid, W. Hofer, and P. Varga. A quantitative LEED analysis of the oxygen-induced p(3 x 1) reconstruction of Pt25Rh75(100). *Surface Science*, 416(3):384–395, October 1998.

[17] E. L. D. Hebenstreit, W. Hebenstreit, M. Schmid, and P. Varga. Pt25Rh75(111), (110), and (100) studied by scanning tunnelling microscopy with chemical contrast. *Surface Science*, 441(2-3):441–453, November 1999.

[18] Ronald M. Wolf, Jacobus Siera, Falco C. M. J. M. Van Delft, and Bernard E. Nieuwenhuys. A comparative study of the behaviour of single-crystal surfaces and supported catalysts in NO reduction and CO oxidation over Pt-Rh alloys. *Faraday Discussions of the Chemical Society*, 87(1):275–289, January 1989.

[19] P. T. Wouda, M. Schmid, W. Hebenstreit, and P. Varga. Interaction of oxygen with PtRh(100) studied with STM. *Surface Science*, 388(1-3):63–70, October 1997.

[20] P. T. Wouda, B. E. Nieuwenhuys, M. Schmid, and P. Varga. Chemically resolved STM on a PtRh(100) surface. *Surface Science*, 359(1-3):17–22, July 1996.

[21] E. Platzgummer, M. Sporn, R. Koller, S. Forsthuber, M. Schmid, W. Hofer, and P. Varga. Temperature-dependent segregation on Pt Rh (111) and (100). *Surface Science*, 419(1-2):236–248, January 1999.

[22] S. B. Maisel, T. C. Kerscher, and S. Müller. No miscibility gap in Pt-Rh binary alloys: A first-principles study. *Acta Materialia*, 60(3):1093–1098, February 2012.

[23] Jian Zheng, Oleksii Ivashenko, Helmer Fjellvåg, Irene M. N. Groot, and Anja O. Sjåstad. Roadmap for Modeling RhPt/Pt(111) Catalytic Surfaces. *Journal of Physical Chemistry C*, 122(46):26430–26437, November 2018.

[24] Veijo Honkimäki, Paul Tafforeau, and Jonathan Wright. High-Energy Synchrotron Radiation Research at the ESRF. *Synchrotron Radiation News*, 33(6):5–10, January 2020.

[25] Hai-Long Jiang and Qiang Xu. Recent progress in syngergistic catalysis over heterometallic nanoparticles. *Journal of Materials Chemistry*, 21(36):13705–13725, August 2011.

[26] Zhen Guo, Bin Liu, Qinghong Zhang, Weiping Deng, Ye Wang, and Yanhui Yang. Recent advances in heterogeneous selective oxidation catalysis for sustainable chemistry. *Chemical Society Reviews*, 43(10):3480–3524, February 2014.

[27] Z. Hussein, W. R. A. Huff, S. A. Kellar, E. J. Moler, P. A. Heimann, W. McKinney, C. Cummings, T. Lauritzen, J. P. McKean, F. J. Palomares, H. Wu, Y. Zheng, A. T. Young, H. A. Padmore, C. S. Fadley, and D. A. Shirley. High-resolution beamline 9.3.2 in the energy range 30-1500 eV at the Advanced Light Source: Design and performance. *Review of Scientific Instruments*, 67(9):3372–1–3372–4, September 1996.

[28] Michael E. Grass, Patrik G. Karlsson, Funda Aksoy, Måns Lundqvist, Björn Wannberg, Bongjin S. Mun, Zahid Hussein, and Zhi Liu. New ambient pressure photoemission endstation at Advanced Light Source beamline 9.3.2. *Review of Scientific Instruments*, 81(5):053106, May 2010.

[29] Rui Chang, Young Pyo Hong, Stephanus Axnanda, Boahua Mao, Naila Jabeen, Suidong Wang, Renzhong Tai, and Zhi Liu. In-situ photoelectron spectroscopy with online activity measurement for catalysis research. *Current Applied Physics*, 12(5):1292–1296, September 2012.

[30] Martin Prutton. *Introduction to Surface Physics*. Oxford University Press, 1994.

[31] I. Chorkendorff and J. W. Niemantsverdriet. *Concepts of Modern Catalysis and Kinetics*. Wiley, third edition, 2013.

[32] Donald R. Askeland and Pradeep P. Fulay. *Essentials of Materials Science and Engineering*. CENGAGE Learning, second edition, 2010.

[33] Gary Attard and Colin Barnes. *Surfaces*. Oxford Science Publications, first edition, 1998.

[34] B. L. M. Hendriksen, S. C. Bobaru, and J. W. M. Frenken. Oscillatory CO oxidation on Pd(1 0 0) studied with in situ scanning tunneling microscopy. *Surface Science*, 552(1-3):229–242, March 2004.

[35] Elizabeth A. Wood. Vocabulary of Surface Crystallography. *Journal of Applied Physics*, 35(4):1306–1312, April 1964.

[36] Natalia M. Martin, Maxime Van Den Bossche, Anders Hellman, Henrik Grönbeck, Can Hakanoglu, Johan Gustafson, Sara Blomberg, Niclas Johansson, Zhi Liu, Stephanus Axnanda, Jason F. Weaver, and Edvin Lundgren. Intrinsic ligand effect governing the catalytic activity of Pd oxide thin films. *ACS Catalysis*, 4(10):3330–3334, October 2014.

[37] Vikram Mehar, Minkyu Kim, Mikhail Shipilin, Maxime Van Den Bossche, Johan Gustafson, Lindsay R. Merte, Uta Hejral, Henrik Grönbeck, Edvin Lundgren, Aravind Asthagiri, and Jason F. Weaver. Understanding the Intrinsic Surface Reactivity of Single-Layer and Multilayer PdO(101) on Pd(100). *ACS Catalysis*, 8(9):8553–8567, September 2018.

[38] Mikhail Shipilin, Uta Hejral, Edvin Lundgren, Lindsay R. Merte, Chu Zhang, Andreas Stierle, Uta Ruett, Olof Gutowski, Magnus Skoglundh, Per Anders Carlsson, and Johan Gustafson. Quantitative surface structure determination using in situ high-energy SXRD: Surface oxide formation on Pd(100) during catalytic CO oxidation. *Surface Science*, 630:229–235, December 2014.

[39] Mikhail Shipilin, Andreas Stierle, Lindsay R. Merte, Johan Gustafson, Uta Hejral, Natalia M. Martin, Chu Zhang, Dirk Franz, Volkan Kilic, and Edvin Lundgren. The influence of incommensurability on the long-range periodicity of the Pd(100)-(5×5)R27°-PdO(101). *Surface Science*, 660:1–8, June 2017.

[40] Feng Zhang, Li Pan, Tao Li, John T. Diulus, Aravind Asthagiri, and Jason F. Weaver. CO oxidation on PdO(101) during temperature-programmed reaction spectroscopy: Role of oxygen vacancies. *Journal of Physical Chemistry C*, 118(49):28647–28661, December 2014.

[41] Jason F. Weaver, Feng Zhang, Li Pan, Tao Li, and Aravind Asthagiri. Vacancy-mediated processes in the oxidation of CO on PdO(101). *Accounts of Chemical Research*, 48(5):1515–1523, May 2015.

[42] Jason F. Weaver, Juhee Choi, Vikram Mehar, and Chengjun Wu. Kinetic coupling among metal and oxide phases during CO oxidation on partially reduced PdO(101): Influence of gas-phase composition. *ACS Catalysis*, 7(10):7319–7331, October 2017.

[43] Edvin Lundgren, Chu Zhang, Lindsay R. Merte, Mikhail Shipilin, Sara Blomberg, Uta Hejral, Jianfeng Zhou, Johan Zetterberg, and Johan Gustafson. Novel in Situ Techniques for Studies of Model Catalysts. *Accounts of Chemical Research*, 50(9):2326–2333, September 2017.

[44] Harald Ibach. *Physics of Surfaces and Interfaces*. Springer-Verlag Berlin Heidelberg, 2006.

[45] Chapter 7 Oxygen on Oxides. In Harold H. Kung, editor, *Transition Metal Oxides*, volume 45 of *Studies in Surface Science and Catalysis*, pages 110–120. Elsevier, 1989.

[46] Irving Langmuir. The mechanism of the catalytic action of platinum in the reactions 2CO + O2 = 2CO2 and 2H2 + O2 = 2H2O. *Transactions of the Faraday Society*, 17:621–654, January 1922.

[47] Cyril Norman Hinshelwood. The kinetics of the interactions of nitrous oxide and hydrogen. *The Royal Society*, 106(737):292–298, September 1924.

[48] D. D. Eley and E. K. Rideal. Parahydrogen Conversion on Tungsten. *Nature*, 146(3699):401–402, September 1940.

[49] P. Mars and D. W. van Krevelen. Oxidations carried out by means of vanadium oxide catalysts. *Chemical Engineering Science*, 3:41–59, May 1954. The Proceedings of the Conference on Oxidation Processes.

[50] N. M. Martin, M. Van Den Bossche, H. Grönbeck, C. Hakanoglu, F. Zhang, T. Li, J. Gustafson, J. F. Weaver, and E. Lundgren. CO adsorption on clean and oxidized Pd(111). *Journal of Physical Chemistry C*, 118(2):1118–1128, January 2014.

[51] J. Gustafson, R. Westerström, A. Resta, A. Mikkelsen, J. N. Andersen, O. Balmes, X. Torrelles, M. Schmid, P. Varga, B. Hammer, G. Kresse, C. J. Baddeley, and E. Lundgren. Structure and catalytic reactivity of Rh oxides. *Catalysis Today*, 145(3-4):227–235, July 2009.

[52] P. Marcus. On some fundamental factors in the effect of alloying elements on passivation of alloys. *Corrosion Science*, 36(12):2155–2158, December 1994.

[53] Xuefei Weng, Hongjia Ren, Mingshu Chen, and Huilin Wan. Effect of surface oxygen on the activation of methane on palladium and platinum surfaces. *ACS Catalysis*, 4(8):2598–2604, August 2014.

[54] G. Myhre, D. Shindell, F.-M. Bréon, W. Collins, J. Fuglestvedt, J. Huang, D. Koch, J.-F. Lamarque, D. Lee, B. Mendoza, T. Nakajima, A. Robock, G. Stephens, T. Takemura, and H. Zhang. Anthropogenic and Natural Radiative Forcing. In T. F. Stocker, D. Qin, G.-K. Plattner, M. Tignor, S. K. Allen, J. Boschung, A. Nauels, Y. Xia, V. Bex, and P. M. Midgle, editors, *Climate Change 2013: The Physical Science Basis. Contribution of Working Group I to the Fifth Assessment Report of the Intergovernmental Panel on Climate Change*, chapter 8, pages 659–740. Cambridge University Press, Cambridge, United Kingdom and New York, NY, USA, 2013.

[55] Jaime Wisniak. The History of Catalysis. From the Beginning to Nobel Prizes. *Educación Química*, 21(1):60–69, January 2010.

[56] H. J. Freund, H. Kuhlenbeck, J. Libuda, G. Rupprechter, M. Bäumer, and H. Hamann. Bridging the pressure and materials gaps between catalysis and surface science: Clean and modified oxide surfaces. *Topics in Catalysis*, 15(2-4):201–209, June 2001.

[57] Lesley E. Smart and Elaine A. Moore. *Solid State Chemistry: An Introduction*. Taylor & Francis Group, LLC, third edition, 2005.

[58] R. Westerström, J. G. Wang, M. D. Ackermann, J. Gustafson, A. Resta, A. Mikkelsen, J. N. Andersen, E. Lundgren, O. Balmes, X. Torrelles, J. W.M. Frenken, and B. Hammer. Structure and reactivity of a model catalyst alloy under realistic conditions. *Journal of Physics Condensed Matter*, 20(18):6–12, April 2008.

[59] J. C. Slater. Atomic Radii in Crystals. *Journal of Chemical Physics*, 41(10):3199–3204, November 1964.

[60] E. Clementi, D. L. Raimondi, and W.P. Reinhardt. Atomic Screening Constants from SCF Functions. II. Atoms with 37 to 86 Electrons. *Journal of Chemical Physics*, 47(4):1300–1307, August 1967.

[61] L. Z. Mezey and J. Giber. The Surface Free Energies of Solid Chemical Elements: Calculation from Internal Free Enthalpies of Atomization. *Japanese Journal of Applied Physics*, 21(11R):1569–1571, November 1982.

[62] Science Notes: List of Electronegativity Values of the Elements. `https://sciencenotes.org/`

list-of-electronegativity-values-of-the-elements/. Accessed 2023-08-14.

[63] Andrea Resta, Uta Hejral, Sara Blomberg, Stefano Albertin, Alina Vlad, Yves Garreau, Corentin Chatelier, Federica Venturini, Pilar Ferrer, Georg Held, Dave Grinter, Edvin Lundgren, and Alessandro Coati. Ammonia Oxidation over a Pt25Rh75(001) Model Catalyst Surface: An Operando Study. *Journal of Physical Chemistry C*, 124(40):22192–22199, October 2020.

[64] Rafal J. Wrobel, Stefan Becker, and Helmut Weiss. Influence of subsurface oxygen in the catalytic CO oxidation on Pd(111). *Journal of Physical Chemistry C*, 119(10):5386–5394, March 2015.

[65] Yuji Matsumoto, Yuji Okawa, Takaya Fujita, and Ken Ichi Tanaka. STM studies of a catalytically active p(3 × 1) Pt-Rh(100) alloy surface. *Surface Science*, 355(1-3):109–114, June 1996.

[66] J. Gustafson, A. Mikkelsen, M. Borg, J. N. Andersen, E. Lundgren, C. Klein, W. Hofer, M. Schmid, P. Varga, L. Köhler, G. Kresse, N. Kasper, A. Stierle, and H. Dosch. Structure of a thin oxide film on Rh(100). *Physical Review B - Condensed Matter and Materials Physics*, 71(11):1–9, March 2005.

[67] J. Gustafson, E. Lundgren, A. Mikkelsen, M. Borg, J. Klikovits, M. Schmid, P. Varga, and J. N. Andersen. The Rh(100)-(3×1)-2O structure. *Journal of Physics Condensed Matter*, 24(22):1–4, June 2012.

[68] Petr Kostelník, Nicola Seriani, Georg Kresse, Anders Mikkelsen, Edvin Lundgren, Volker Blum, Tomáš Šikola, Peter Varga, and Michael Schmid. The Pd (1 0 0) - (sqrt(5) × sqrt(5)) R 27 ° s(-) O surface oxide: A LEED, DFT and STM study. *Surface Science*, 601(6):1574–1581, March 2007.

[69] Jutta Rogal, Karsten Reuter, and Matthias Scheffler. Thermodynamic stability of PdO surfaces. *Physical Review B - Condensed Matter and Materials Physics*, 69(7):1–8, February 2004.

[70] Nicola Seriani, Judith Harl, Florian Mittendorfer, and Georg Kresse. A first-principles study of bulk oxide formation on Pd(100). *The Journal of Chemical Physics*, 131(5):054701–1–054701–7, August 2009.

[71] H. L. Abbott, A. Aumer, Y. Lei, C. Asokan, R. J. Meyer, M. Sterrer, S. Shaikhutdinov, and H. J. Freund. CO adsorption on monometallic and bimetallic Au-Pd nanoparticles supported on oxide thin films. *Journal of Physical Chemistry C*, 114(40):17099–17104, July 2010.

[72] Marie Claire Saint-Lager, Marie Angélique Languille, Francisco J. Cadete Santos Aires, Aude Bailly, Stéphanie Garaudee, Eric Ehret, and Odile Robach. Oxygen-Induced Changes of the Au30Pd70(110) Surface Structure and Composition under Increasing O2 Pressure. *Journal of Physical Chemistry C*, 122(39):22588–22596, October 2018.

[73] Jens Als-Nielsen and Des McMorrow. *Elements of Modern X-ray Physics*. Wiley, second edition, 2011.

[74] Weijia Zhang and Robert G Fuller. Nobel prize winners in physics from 1901 to 1990: simple statistics for physics teachers. *Physics Education*, 33(3):196–203, May 1998.

[75] U. Hejral, P. Müller, M. Shipilin, J. Gustafson, D. Franz, R. Shayduk, U. Rütt, C. Zhang, L. R. Merte, E. Lundgren, V. Vonk, and A. Stierle. High-energy x-ray diffraction from surfaces and nanoparticles. *Physical Review B*, 96(19):1–8, November 2017.

[76] Ankit S. Disa, Frederick J. Walker, and Charles H. Ahn. High-Resolution Crystal Truncation Rod Scattering: Application to Ultrathin Layers and Buried Interfaces. *Advanced Materials Interfaces*, 7(6):1–37, March 2020.

[77] Johan Gustafson, Mikhail Shipilin, Chu Zhang, Andreas Stierle, Uta Hejral, Uta Ruett, Olof Gutowski, Per-Anders Carlsson, Magnus Skoglundh, and Edvin Lundgren. High-Energy Surface X-ray Diffraction for Fast Surface Structure Determination. *Science*, 343(6172):758–761, February 2014.

[78] Measurlabs: Grazing incidence X-ray diffraction. `https://measurlabs.com/methods/grazing-incidence-x-ray-diffraction-gixrd/`. Accessed 2023-08-15.

[79] Hiroo Tajiri, Osami Sakata, and Toshio Takahashi. Surface X-ray diffraction in transmission geometry. *Applied Surface Science*, 234(1-4):403–408, July 2004.

[80] Finn Reikowski, Tim Wiegmann, Jochim Stettner, Jakub Drnec, Veijo Honkimäki, Fouad Maroun, Philippe Allongue, and Olaf M. Magnussen. Transmission Surface Diffraction for Operando Studies of Heterogeneous Interfaces. *Journal of Physical Chemistry Letters*, 8(5):1067–1071, March 2017.

[81] Clinton Davisson and Lester H. Germer. Diffraction of Electrons by a Crystal of Nickel. *Physical Review Journals Archive*, 30(6):705–740, December 1927.

[82] N. V. Alov. Fifty Years of X-ray Photoelectron Spectroscopy. *Journal of Analytical Chemistry*, 60(3):297–300, March 2005.

[83] S. Doniach and M. Šunjić. Many-electron singularity in X-ray photoemission and X-ray line spectra from metals. *Journal of Physics C: Solid State Physics*, 3(2):285–291, March 1970.

[84] M. Brun, A. Berthet, and J. C. Bertolini. XPS, AES and Auger parameter of Pd and PdO. *Journal of Electron Spectroscopy and Related Phenomena*, 104(1-3):55–60, July 1999.

[85] S. Kurth, M. A. L. Marques, and E. K. U. Gross. Density-Functional Theory. In Franco Bassani, Gerald L. Liedl, and Peter Wyder, editors, *Encyclopedia of Condensed Matter Physics*, pages 395–402. Elsevier, Oxford, 2005.

[86] Axel Groß. *Theoretical Surface Science - A Microscopic Perspective*. Springer-Verlag Berlin Heidelberg, second edition, 2009.

[87] P. Hohenberg and W. Kohn. Inhomogeneous Electron Gas. *Physical Review*, 136(3B):B864–B871, November 1964.

[88] W. Kohn and L. J. Sham. Self-Consistent Equations Including Exchange and Correlation Effects. *Physical Review*, 140(4A):A1133–A1138, November 1965.

[89] G. Kresse and J. Hafner. Ab initio molecular dynamics for liquid metals. *Physical Review B*, 47(1):558–561, January 1993.

[90] G. Kresse and J. Furthmüller. Efficiency of ab-initio total energy calculations for metals and semiconductors using a plane-wave basis set. *Computational Materials Science*, 6(1):15–50, July 1996.

[91] G. Kresse and J. Furthmüller. Efficient iterative schemes for ab initio total-energy calculations using a plane-wave basis set. *Physical Review B*, 54(16):11169–11186, October 1996.

[92] J. Gustafson, R. Westerström, A. Mikkelsen, X. Torrelles, O. Balmes, N. Bovet, J. N. Andersen, C. J. Baddeley, and E. Lundgren. Sensitivity of catalysis to surface structure: The example of CO oxidation on Rh under realistic conditions. *Physical Review B - Condensed Matter and Materials Physics*, 78(4):1–6, July 2008.

[93] J. Gustafson, A. Mikkelsen, M. Borg, E. Lundgren, L. Köhler, G. Kresse, M. Schmid, P. Varga, J. Yuhara, X. Torrelles, C. Quirós, and J. N. Andersen. Self-Limited Growth of a Thin Oxide Layer on Rh(111). *Physical Review Letters*, 92(12):126102–1–126102–4, March 2004.

[94] O. M. Løvvik. Surface segregation in palladium based alloys from density-functional calculations. *Surface Science*, 583(1):100–106, May 2005.

[95] Elias Vlieg. *ROD*: a program for surface X-ray crystallography. *Journal of Applied Crystallography*, 33(2):401–405, April 2000.

[96] Daniel M. Kamiński. WinRod. `https://dkami.umcs.pl/programs/winrod/`, 2020. Accessed 2023-10-24.

[97] H. Okamoto and T. B. Massalski. The Au–Pd (Gold-Palladium) system. *Bulletin of Alloy Phase Diagrams*, 6(3):229–235, June 1985.

[98] Tongyu Wang, Baihai Li, Jianhui Yang, Hong Chen, and Liang Chen. First principles study of oxygen adsorption and dissociation on the Pd/Au surface alloys. *Physical Chemistry Chemical Physics*, 13(15):7112–7120, April 2011.

Printed by Media-Tryck, Lund 2023 NORDIC SWAN ECOLABEL 3041 0903

About the author

HELEN EDSTRÖM was born in Ängelholm where she grew up developing an interest in natural science. In 2009, she moved to Lund to study at Lund Institute of Technology, from where she holds a Master in Engineering Nanoscience. When she does not do scientific stuff, she enjoys reading, gaming, working out, spending time with friends, and writing fantasy. One of her biggest challenges during her time as a PhD student was to overcome a depression.

LUND UNIVERSITY

Faculty of Science
Department of Physics

ISBN 978-91-8039-832-9